Current state of nuclear matter calculations

B. D. Day

*Argonne National Laboratory, Argonne, Illinois 60439**

The current state of nuclear matter calculations is described with special reference to the present disagreement between the variational and Brueckner–Bethe methods. The system is assumed to consist of point nucleons with a nonrelativistic Hamiltonian containing the kinetic energy and two-body potentials. The physical ideas of the variational method, especially of its hypernetted-chain version, and of the Brueckner—Bethe method are outlined. Practical ways of testing the validity of these methods are discussed and are illustrated by numerical results taken from the literature. It is found for central forces that the hypernetted-chain variational method, if properly used, gives reliable upper bounds to the ground-state energy. Lowest-order Brueckner–Bethe results lie well above these upper bounds, and it is both important and feasible to check whether higher-order corrections will bring the Brueckner–Bethe results into agreement with the variational ones. For realistic nuclear potentials, which have tensor forces, spin–orbit forces, etc., the situation is much less clear. An adequate calculation has not yet been done by either the variational or Brueckner–Bethe method. For the Reid potential, with the presently available numerical results, the variational calculation predicts a much higher saturation density than the Brueckner–Bethe calculation. Feasible calculations that will help to resolve this discrepancy are discussed.

CONTENTS

I. INTRODUCTION

The simplest model of a nucleus is a collection of point nucleons that obey the nonrelativistic Schrödinger equation and interact through a two-body potential that fits nucleon–nucleon scattering data and the properties of the deuteron. There are several reasons for studying this model: (1) It provides a test of proposed nucleon–nucleon potentials. A potential that fits the scattering data and deuteron properties but predicts wrong binding energies and density distributions for heavier nuclei can be thrown out. (2) If a satisfactory potential can be found, this will greatly help to unify nuclear physics. Basic properties of nuclei and nucleon–nucleon scattering would then be understood in terms of the *same* underlying two-body force. (3) If no satisfactory potential can be found, the results may give a clue about the importance of interesting effects not included in the model, e.g., many-body forces, meson degrees of freedom, etc.

The first requirement for any two-body potential (besides fitting the scattering data and deuteron properties) is that it correctly reproduce the saturation point of nuclear matter. Nuclear matter is a system of nucleons at uniform density that approximates conditions in the interior of a heavy nucleus. The energy per particle is a function of the density ρ (or, equivalently, of the Fermi momentum k_F, where $\rho = 2k_F^3/3\pi^2$), and the minimum of this curve defines the saturation point. The empirical saturation point is deduced by extrapolation from finite nuclei, using either the liquid-drop model and semiempirical mass formula (Myers and Swiatecki, 1969) or Hartree–Fock calculations with phenomenological forces fitted to finite nuclei (Negele, 1970; Campi and Sprung, 1972; Fái and Németh, 1973). The resulting empirical saturation point has an energy per particle between −15 and −17 MeV and a Fermi momentum k_F in the range 1.29–1.44 fm^{-1}. Any assumed two-body potential implies a curve of energy per particle versus density for nuclear matter. The saturation point of this curve must agree with the empirical one if the potential is to account for the properties of nuclei. Therefore it is essential to have a method for reliably calculating, for an assumed potential, the binding energy of nuclear matter as a function of density. Only if this calculation can be done accurately does it make sense to compare the calculated saturation point with the empirical one and hence to accept or reject the potential.

In spite of much effort, our ability to make these calculations is still in doubt. Until two years ago it was generally believed that the Brueckner–Bethe method (Bethe, 1971; Day, 1967; Sprung, 1972; Köhler, 1975; Jeukenne *et al.*, 1976) was adequate. Earlier work by the Clark group (Bäckman *et al.*, 1972), which showed a discrepancy between Brueckner–Bethe and variational results for a central force, had not been followed up. But two years ago Pandharipande and Wiringa (1976) found similar results for the potential of Reid (1968), which was believed to be the best available nucleon–nucleon potential. They also concluded that the Reid potential saturates at a density much higher than that

*Work performed under the auspices of the Department of Energy.

Copyright ©1978 American Physical Society

obtained in Brueckner–Bethe calculations (and also much higher than the empirical saturation density). Since then the variational method has been under intensive development, and it has been suggested that the usual formulation of the Brueckner–Bethe method is unreliable. The result has been a very healthy re-examination of the nuclear matter problem. In this paper I try to give a balanced account of the present situation. A definitive picture has not yet emerged. But a number of important facts have been definitely established, and these suggest calculations that will further clarify the situation.

In this paper we are concerned with the validity of different methods of calculation, so we always assume that the nucleons obey the nonrelativistic Schrödinger equation with a Hamiltonian consisting of kinetic energies and two-body potentials, i.e.,

$$H=\sum_{i=1}^{A} T_i+\sum_{i<j}^{A} v_{ij}, \tag{1.1}$$

where A is the number of nucleons. The possible importance of many-body forces, relativistic effects, etc. is not considered.

Since variational calculations using the hypernetted-chain method have been introduced only recently into nuclear physics, we describe this method in more detail than the Brueckner–Bethe method, whose application to nuclear physics has been reviewed before (Day, 1967; Bethe, 1971; Sprung, 1972; Köhler, 1975; Jeukenne *et al.*, 1976). Our aim is to assess the reliability of different methods of calculation and from the vast literature we quote those numerical results that are most relevant for this purpose. The variational method is discussed in Sec. II, with bosons, fermions with central forces, and fermions with tensor forces considered in order of increasing complexity. The Brueckner–Bethe method is described in Sec. III, and further discussion and comparison of the methods is given in Sec. IV.

II. VARIATIONAL METHOD

A. Introduction

In the variational method, one chooses a trial many-body wave function of the form

$$\Psi=F\Phi \tag{2.1}$$

and attempts to evaluate

$$E_{\rm var}=A^{-1}\frac{\langle\Phi|F^{\dagger}HF|\Phi\rangle}{\langle\Phi|F^{\dagger}F|\Phi\rangle}, \tag{2.2}$$

which is an upper bound for the ground-state energy per particle. Here, Φ is the noninteracting Fermi-gas wave function for fermions, and $\Phi=1$ for bosons.

When the two-body potential $v(r)$ is simply a function of r, the correlation operator F is usually chosen to be multiplication by a product of two-body correlation functions $f(r_{ij})$,

$$F=\prod_{i<j}^{A} f(r_{ij}). \tag{2.3}$$

The function $f(r_{ij})$ must go to zero at small r_{ij} because the two-body potential is strongly repulsive there. At large r_{ij}, $f(r_{ij})$ is required to approach unity. Several such correlation functions are plotted in Fig. 1.

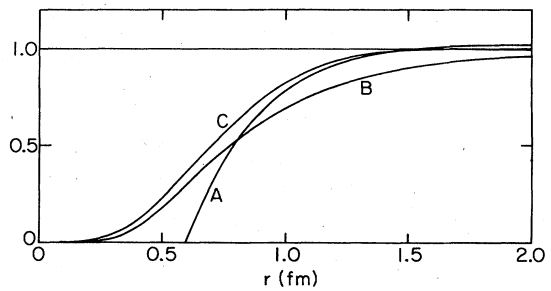

FIG. 1. Typical correlation functions $f(r)$ for nuclear matter with central forces. Curve A is defined by Eq. (2.32) with $c=0.6$ fm, $\mu=1.5$ fm^{-1}, $\gamma=1.346$. It has been used by Chakkalakal (1976) for the OMY potential of Eqs. (2.45) and (2.46) at $k_F=1.8$ fm^{-1}. Curve B is defined by Eq. (2.33) with $A=2.0$ fm, $B=1.7$ fm^{-1}, $D=0.08$ fm. It was used by Ceperley (1977) for the potential v_2 of Eq. (2.47) at $k_F=1.79$ fm^{-1} ($\rho=0.386$ fm^{-3}). Curve C is the solution of Eq. (2.34) for potential v_2 with $k_F=1.8$ fm^{-1} and $d=2r_0$, where $r_0=0.84$ fm.

For the nuclear two-body potential, which has tensor forces, spin–orbit forces, etc., the correlation operator (2.3) would also give an upper bound to the energy. However, this upper bound would presumably be too far above the exact ground-state energy to be useful. For example, the expectation value of the tensor force, which is known to be very important for nuclear binding, would be exactly zero for the correlation operator (2.3). Thus for the nuclear force Eq. (2.3) must be generalized. One possible generalization is (Pandharipande and Wiringa, 1976)

$$F=\mathcal{S}\prod_{i<j}^{A} f_{ij}, \tag{2.4}$$

where $\mathcal{S}$ is the symmetrizer for A particles, and f_{ij} is a quite general two-body operator that builds in, for example, tensor correlations. The different f_{ij} do not commute with each other, and this is why the product (2.4) must be symmetrized.

In general the correlation operator F must have the cluster property, i.e., it must decompose into two commuting factors,

$$F_A\to F_m F_{A-m}, \tag{2.5}$$

when any set of m particles is spatially well separated from the others. For a given A-body correlation operator F_A, Eq. (2.5) defines correlation operators F_m for clusters of $2,3,\ldots,A-1$ particles. By definition, the one-body correlation operator is unity. Also, we usually denote the two-body correlation operator by f rather than F_2, which is consistent with Eqs. (2.3) and (2.4). For any correlation operator with the cluster property, a variety of cluster expansions for $E_{\rm var}$ can be developed (Clark and Westhaus, 1968). In the Van Kampen cluster expansion (Van Kampen, 1961; Clark and Westhaus, 1968; Clark and Ristig, 1973), which is the one usually used in numerical calculations, the nth order approximation to $E_{\rm var}$ is given in terms of correlation operators F_k for clusters of $k=2,3,\ldots,n$ particles.

The correlation operator F should be sufficiently flexible that $E_{\rm var}$ is close to the ground-state energy but simple enough that $E_{\rm var}$ can be accurately evaluated.

Equation (2.3) is presumably the simplest possible choice that goes to zero whenever any pair of particles is close together, as required by the strong short-range repulsion in the potential. But when the f_{ij} do not all commute, simpler choices than Eq. (2.4) can be found, and this possibility should be kept in mind. One example (Ristig *et al.*, 1972) is discussed in Sec. II.D.

In any calculation, the two important questions are as follows: (1) How accurately can the expectation value $E_{\rm var}$ be calculated? (2) How far above the ground-state energy is the expectation value? If the expectation value could be calculated exactly for the wave function (2.3) or (2.4), we could vary the two-body correlation operator f to minimize the energy. However, the expectation value can only be calculated approximately, and any approximation method makes use of the properties of f. Therefore, when f is varied to minimize the energy, it is crucial that f be restricted so that the approximation used to evaluate $E_{\rm var}$ remains valid.

For example, cluster expansion calculations, which usually include two- and three-body terms, must be constrained to keep f within the space of functions for which the cluster expansion is reasonable (Clark and Ristig, 1972). In particular, the range of f must be small enough that correlations among more than three particles are negligible. More powerful approximation schemes, such as the hypernetted-chain (HNC) and Monte Carlo methods, will be valid for a larger class of f's than will the cluster expansion. But there will be f's for which these methods also break down. Generally speaking, in any variational calculation, it is essential to guard against the use of correlation operators for which the chosen approximation for calculating $E_{\rm var}$ breaks down.

The complexity needed in f depends on the two-body potential. For a central potential that is independent of spin and parity, f can be taken to be simply a function of the distance r between two particles. In this case, we will see that the cluster expansion, as well as the more powerful Monte Carlo and HNC methods, can be used to evaluate the expectation value with high accuracy for potentials and densities appropriate to nuclear matter. For realistic phenomenological nuclear forces, which are strongly spin and isospin dependent and have strong tensor forces, f must contain the tensor operator and other operators. The HNC and Monte Carlo methods, as presently formulated, are then not available. Consequently, the accuracy of the calculated expectation value is much less certain, especially at densities much higher than the empirical saturation density of nuclear matter.

In Sec. II.B, we introduce the HNC approximation and the cluster expansion for the simplest case—a system of interacting bosons. In Sec. II.C these ideas are applied to Fermi systems with central forces. The recent fermion Monte Carlo calculations (Ceperley *et al.*, 1977) are also discussed. Section II.D treats the more difficult case of tensor and state-dependent forces.

B. Bosons

By studying the Bose system, we can understand the physical ideas of the cluster expansion and of the hypernetted-chain (HNC) method without the complication of antisymmetry. We assume the two-body potential to be a function $v(r)$, and we use the correlation operator (2.3). Putting $\Phi = 1$ in Eq. (2.1) gives the variational wave function in the form

$$\Psi = \prod_{i<j} f(r_{ij}) . \tag{2.6}$$

The two-body distribution function $g(r)$ is defined by

$$g(r_{12}) = \frac{A(A-1)/\rho^2 \int d\mathbf{r}_3 \cdots d\mathbf{r}_A |\Psi|^2}{\langle \Psi | \Psi \rangle} , \tag{2.7}$$

where ρ is the density and A is the number of particles. Given that there is a particle at $\mathbf{r} = 0$, $g(r)d\tau$ is the probability of finding a particle in volume element $d\tau$ at a distance r from the point $\mathbf{r} = 0$. One then finds the expectation value of the potential energy per particle V to be

$$V = \tfrac{1}{2}\rho \int g(r) v(r)\, d^3r . \tag{2.8}$$

To calculate $g(r)$, we use the formula

$$g(r_{12}) = f^2(r_{12})[1 + D(r_{12})] , \tag{2.9}$$

where $D(r_{12})$ is given by an infinite series whose terms are represented by linked, irreducible diagrams (van Leeuwen *et al.*, 1959). The basic quantity in this expansion is the short-ranged function $h(r)$ defined by

$$h(r) = f^2(r) - 1 . \tag{2.10}$$

Note that $h(r) \to 0$ for large r.

We illustrate the rules for diagrams by considering two examples, called C_3 and E, that are shown in Figs. 2 and 3, respectively. Their contributions to $D(r_{12})$ are

$$C_3(r_{12}) = \rho \int d\tau_3 h(r_{13}) h(r_{32}) , \tag{2.11}$$

$$E(r_{12}) = \tfrac{1}{2}\rho^2 \int d\tau_3 d\tau_4 h(r_{13}) h(r_{14}) h(r_{34}) h(r_{32}) h(r_{42}) . \tag{2.12}$$

The coordinates $\mathbf{r}_1$ and $\mathbf{r}_2$ are represented in the diagrams by the *external* points labeled 1 and 2 and are not integrated over. The coordinates $\mathbf{r}_3, \mathbf{r}_4, \ldots$, represented by the *internal* points $3, 4 \ldots$, *are* integrated over. Each internal point gives a factor ρ, and each line joining points i and j gives a factor $h(r_{ij})$. The symmetry number $\frac{1}{2}$ in Eq. (2.12) for $E(r_{12})$ occurs because interchanging $\mathbf{r}_3$ and $\mathbf{r}_4$ leaves the integrand unchanged in (2.12) (van Leeuwen *et al.*, 1959).

The quantity $D(r_{12})$ is equal to the sum of the contributions from all linked, irreducible diagrams. A linked diagram is one that consists of a single connected part. An irreducible diagram is one that is not

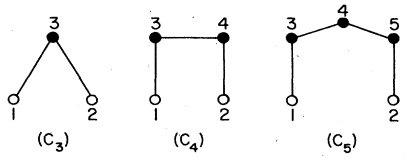

FIG. 2. Chain diagrams for bosons.

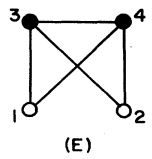

FIG. 3. The simplest boson diagram that is omitted from the hypernetted-chain approximation.

reducible, where a reducible diagram is one that can be cut at one point (called a point of articulation) into two disjoint pieces, with one piece containing only internal points. Figure 4 shows a reducible diagram with a point of articulation at 3. [But diagram C_3 of Fig. 2 is irreducible: if it is cut at point 3, each of the resulting pieces contains an external point.]

Grouping the diagrams according to the number of internal points is equivalent to applying the Van Kampen cluster expansion (Van Kampen, 1961; Clark and Westhaus, 1968; Clark and Ristig, 1973). Putting $D(r_{12})=0$ in Eq. (2.9) gives the two-body cluster approximation $g(r_{12})=f^2(r_{12})$. The first correction to this comes from the three-body term $C_3(r_{12})$. To get an idea of its size, we put $r_{12}=0$ and find from Eq. (2.11)

$$C_3(r_{12}=0)=\rho\int[f^2(r)-1]^2d\tau\,. \tag{2.13}$$

If this is small compared to 1, then the three-body term is small compared to the two-body term. We then expect terms involving four particles to be even smaller, and so on. Thus if Eq. (2.13) is small compared to 1, the cluster expansion, in which the diagrams are grouped according to the number of interacting particles, should work well. This requires that $f(r)$ differ appreciably from 1 over a volume small compared to the volume per particle. A similar condition is necessary for the validity of presently available versions of the Brueckner–Bethe expansion (Brandow, 1966; Day, 1967).

However, one can greatly improve on the cluster expansion because the simple structure of the diagram expansion allows extensive partial summations. We now outline the partial summations that lead to the HNC approximation (van Leeuwen *et al.*, 1959).

Consider the sequence of *chain* diagrams shown in Fig. 2. Their contributions are [note that the subdiagram 342 of C_4, when integrated over $\mathbf{r}_4$, gives $C_3(r_{32})$]

$$C_3(r_{12})=\rho\int h(r_{13})h(r_{32})d\tau_3\,,$$

$$C_4(r_{12})=\rho\int h(r_{13})C_3(r_{32})d\tau_3\,,$$

$$C_n(r_{12})=\rho\int h(r_{13})C_{n-1}(r_{32})d\tau_3\,. \tag{2.14}$$

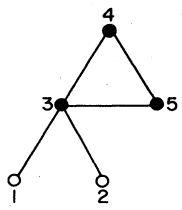

FIG. 4. A reducible boson diagram.

Defining $C(r_{12})$ by

$$C(r_{12})=\sum_{n=3}^{\infty}C_n(r_{12})\,, \tag{2.15}$$

we sum Eqs. (2.14) to get

$$C(r_{12})=\rho\int h(r_{13})[h(r_{32})+C(r_{32})]d\tau_3\,. \tag{2.16}$$

For a given $f(r)$, we can solve this linear integral equation to obtain the sum $C(r)$ of all chain diagrams.

Having $C(r)$, we construct *composite* chain diagrams by connecting the external points 1 and 2 by two or more single chains, as in Fig. 5. Note that in Fig. 5, the integration over $\mathbf{r}_5$ is completely independent of the integrations over $\mathbf{r}_3$ and $\mathbf{r}_4$. Hence the contribution of Fig. 5, and, indeed, of any composite chain diagram, is a product of contributions from single chains. Using this fact, we find that the sum of *all* chain diagrams, both single and composite, is e^C-1. The power series expansion of this formula gives C as its first term. The second term $C^2/2!$ gives all diagrams with two independent chains, such as the one in Fig. 5. The 1342 chain comes from one factor C and the 152 chain from the second factor C. The factor $\frac{1}{2}$ is needed for two reasons. First, if the two independent chains have different numbers of points, as in Fig. 5, their product occurs in C^2 with coefficient 2 and the factor $\frac{1}{2}$ reduces this to the correct coefficient of 1. Second, if the two chains have the same number of points, their product occurs only once in C^2, but the factor $\frac{1}{2}$ is again needed because the symmetry number of the resulting diagram is $\frac{1}{2}$. Continuing to reason in this way, we see that e^C-1 generates all diagrams with one or more independent chains connecting the external points 1 and 2.

We have now summed all diagrams in which the external points 1 and 2 are connected by any number of chains, all of whose links are given by $h(r_{ij})$. The next step is to construct chains from more complicated links, thus obtaining *hypernetted* chains. The links $L(r_{ij})$ that we now have available are

$$L_1(r_{ij})=h(r_{ij})\,, \tag{2.17}$$

$$L_2(r_{ij})=\exp C(r_{ij})-C(r_{ij})-1\,, \tag{2.18}$$

$$L_3(r_{ij})=h(r_{ij})[\exp C(r_{ij})-1]\,. \tag{2.19}$$

The simple link L_1 has already been used to construct C. The link L_2 contains all links made from composite chain diagrams. For example, Fig. 5 contributes to $L_2(r_{12})$. Links made from single chains are not included in L_2 because single-chain diagrams are generated by the link L_1. That is why $C(r_{ij})$ is subtracted in (2.18). But a single chain with a link h is an acceptable link, as is any composite chain with a link h. These terms comprise the link L_3.

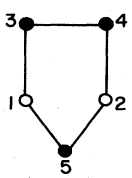

FIG. 5. A composite chain diagram.

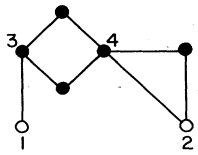

FIG. 6. A chain diagram made from the three types of link defined by Eqs. (2.17)–(2.19).

The link $L(r_{ij})$ used in the next set of chain diagrams is the sum of L_1, L_2, and L_3. Recalling $h = f^2 - 1$, we find

$$L(r_{ij}) = f^2(r_{ij}) \exp C(r_{ij}) - C(r_{ij}) - 1 . \tag{2.20}$$

We can now repeat the process of summing chain diagrams, except that the basic link in each chain is not $h(r_{ij})$ but $L(r_{ij})$. Figure 6 shows a single-chain diagram made from three of these links. Link 13 is of type L_1, namely, $h(r_{13})$. Link 34 is of type L_2, and link 42 is of type L_3. The new set of single-chain diagrams is obtained by solving Eq. (2.16) for C, with h replaced by L. The composite chain diagrams made from the new single chains are then included by replacing C by $e^C - 1$. And putting C into (2.20) gives the links to be used in building still more complicated chains.

Let us imagine that we continue this process indefinitely. The complexity of the diagrams increases very rapidly. But the computations needed at each stage of the process are simple: We need only carry out the following two steps:

(1) Use $C(r_{ij})$ from the preceding stage to get a new link $L(r_{ij})$ from Eq. (2.20).

(2) Use this new link $L(r_{ij})$ to obtain a new $C(r_{ij})$ by solving the equation

$$C(r_{12}) = \rho \int L(r_{13})[L(r_{32}) + C(r_{32})]\, d\tau_3 . \tag{2.21}$$

After the process has converged, L and C will satisfy Eqs. (2.20) and (2.21). Our approximation to the sum of all diagrams $D(r_{12})$ is $\exp[C(r_{12})] - 1$ which, when put into (2.9), gives

$$g(r_{12}) = f^2(r_{12}) \exp[C(r_{12})] . \tag{2.22}$$

Solving (2.20) and (2.22) for L and C in terms of f and g, we substitute the results into (2.21) to get

$$\ln[g(r_{12})/f^2(r_{12})] = \rho \int (g(r_{13}) - \ln[g(r_{13})/f^2(r_{13})] - 1)(g(r_{32}) - 1)\, d\tau_3 . \tag{2.23}$$

This is the HNC equation (van Leeuwen *et al.*, 1959). For a given correlation function $f(r)$, it is a nonlinear integral equation for the two-body distribution function $g(r)$. The solution includes the huge class of diagrams generated in the way described above. Numerical solution of the HNC equation is relatively simple (Pandharipande and Bethe, 1973; Zabolitzky, 1977).

The question arises of whether this particular partial summation is a sensible one. That it *is* sensible can be made plausible as follows. The first diagram omitted from HNC is diagram E of Fig. 3. Let us compare its contribution to that of the chain diagram C_4 of Fig. 2. Diagram E has two more bonds than C_4, and each bond gives the short-ranged function $h(r_{ij})$. Therefore, when we integrate over $\mathbf{r}_3$ and $\mathbf{r}_4$, the integrand for diagram C_4 will be appreciable over a much larger region than the integrand for diagram E. Thus it is plausible that diagrams with the fewest possible bonds will be the largest. These are precisely the diagrams that are summed by the HNC equation.

An instructive numerical example is given by Pandharipande and Bethe (1973) for liquid ^{4}He. They consider a case in which the chain contributions $C_3(r)$, $C_4(r)$, ... form a diverging series. In spite of this, the contribution from diagram E is very small, and solving the HNC equation gives an accurate result for $g(r)$. Thus HNC is accurate at much higher densities than is the cluster expansion.

One can go beyond HNC by evaluating diagram E, which can then be incorporated as a link in the chains generated by the HNC procedure (van Leeuwen, 1959). This gives the HNC/4 approximation (Pandharipande and Bethe, 1973; Smith, 1976; Zabolitzky, 1977; 1976a), which is the first step beyond HNC of a systematic procedure that eventually sums all diagrams. So HNC is not only an intelligent partial summation, but also the first step of a systematic approximation scheme. Numerical evidence for its accuracy will be given in the next subsection, where fermions are discussed. For bosons, HNC has long been used to study liquid ^{4}He and other monatomic liquids. Pandharipande and Schmidt (1977) have recently applied the method to a wide range of interesting Bose systems.

We have seen that the expectation value of the potential energy can be calculated from $g(r)$, and that we can approximate $g(r)$ either by the cluster expansion [if Eq. (2.13) is sufficiently small] or, preferably, by the HNC method. Let us now turn to the kinetic energy. Its expectation value (per particle) can be obtained from either of the formulas

$$T_{\rm PB} = -\hbar^2/2M\langle\Psi|\Psi\rangle^{-1} \int \Psi \nabla_1^2 \Psi\, d\mathbf{r}_1 \cdots d\mathbf{r}_A , \tag{2.24}$$

$$T_{\rm JF} = -\hbar^2/4M\langle\Psi|\Psi\rangle^{-1} \int [\Psi \nabla_1^2 \Psi - (\nabla_1\Psi)^2]\, d\mathbf{r}_1 \cdots d\mathbf{r}_A . \tag{2.25}$$

Integration by parts shows that these two expressions are equal. The first expression gives, upon manipulation, the Pandharipande–Bethe formula (Pandharipande and Bethe, 1973), and the second gives the Jackson–Feenberg formula (Jackson and Feenberg, 1961). As they stand, both formulas are exact. But when one uses a practical approximation scheme, such as the truncated cluster expansion or the HNC method, the two formulas will usually give different results. Far from being a drawback, this fact is extremely useful because the difference between the two approximate kinetic energies gives an idea of the error in the calculation.

Consider first the PB method. Using Eq. (2.6) for Ψ, we find that $\nabla_1^2\Psi$ contains terms such as

$$A = \nabla_1^2 f(r_{12})/f(r_{12})\Psi , \tag{2.26}$$

$$B = \nabla_1 f(r_{12}) \cdot \nabla_1 f(r_{13})/f(r_{12}) f(r_{13})\Psi . \tag{2.27}$$

Multiplying term A by Ψ and integrating over all particles except 1 and 2, we find a result involving the two-body distribution function $g(r_{12})$, and we have already seen how to evaluate $g(r_{12})$. Multiplying term B by Ψ, we integrate over all particles except 1, 2, 3 and obtain a formula containing the three-body distribution function $g_3(\mathbf{r}_1, \mathbf{r}_2, \mathbf{r}_3)$ defined by

$$g_3(\mathbf{r}_1, \mathbf{r}_2, \mathbf{r}_3) = \frac{A(A-1)(A-2)/\rho^3 \int \Psi^2 d\mathbf{r}_4 \cdots d\mathbf{r}_A}{\langle \Psi | \Psi \rangle} . \tag{2.28}$$

There is a diagram expansion for g_3, and partial summations similar to the HNC approximation for $g(r)$ can be carried out. In this HNC approximation for g_3, the superposition approximation is valid, i.e., we have

$$g_3(\mathbf{r}_1, \mathbf{r}_2, \mathbf{r}_3) = g(r_{12}) g(r_{13}) g(r_{23}) . \tag{2.29}$$

Having obtained $g(r)$ by solving the HNC equation, one uses this last formula for g_3 in order to evaluate $T_{\rm PB}$. However, if one goes beyond HNC and evaluates $g(r)$ in the HNC/4 approximation, the superposition approximation (2.29) for g_3 no longer holds. It is then necessary to study separately the diagram expansion for g_3 (Smith, 1976; Zabolitzky, 1977).

We next consider the JF formula (2.25). The terms from $\Psi \nabla_1^2 \Psi$ that require knowledge of $g_3(\mathbf{r}_1, \mathbf{r}_2, \mathbf{r}_3)$ are exactly canceled by similar terms from $(\nabla_1 \Psi)^2$. Hence only $g(r)$ is needed to evaluate $T_{\rm JF}$. The final expressions used for computation in the two methods are

$$T_{\rm PB} = -\frac{\hbar^2}{2M} \rho \int g(r) \frac{\nabla^2 f}{f} d\tau - \frac{\hbar^2}{2M} \rho^2 \int g_3(\mathbf{r}_1, \mathbf{r}_2, \mathbf{r}_3) \frac{\nabla_1 f(r_{12}) \cdot \nabla_1 f(r_{13})}{f(r_{12}) f(r_{13})} d\tau_2 d\tau_3 , \tag{2.30}$$

$$T_{\rm JF} = \frac{\hbar^2}{4M} \rho \int g(r) \left[-\frac{\nabla^2 f}{f} + \left(\frac{\nabla f}{f} \right)^2 \right] d\tau . \tag{2.31}$$

Having formulas for the energy expectation value, we consider the choice of the correlation function $f(r)$. This choice depends rather little on whether the particles are bosons or fermions. The two methods in most common use are the following: (1) Choose an analytic form for f that contains parameters and adjust the parameters to minimize the energy. (2) Solve the Pandharipande differential equation for f (Pandharipande and Wiringa, 1976; Pandharipande and Bethe, 1973). Let us consider these two methods in turn.

A two-parameter form used by the Clark group (Chakkalakal *et al.*, 1976) for a potential with a hard core of radius c is

$$f(r) = 0, \quad r < c$$
$$= (1 - e^{-\mu(r-c)})(1 + \gamma e^{-\mu(r-c)}), \quad r > c . \tag{2.32}$$

For a given value of μ, γ is adjusted to satisfy the angle-average Pauli condition [see Eq. (2.40)]. This condition is helpful in restricting $f(r)$ to that class of functions for which the cluster expansion is useful. The value of μ is then adjusted numerically to minimize the energy. Equation (2.32) is plotted for typical parameter values in Fig. 1.

An analytic form used in Monte Carlo calculations (Ceperley *et al.*, 1977) and discussed further in Sec. II.C is

$$f(r) = \exp[-(A/r) e^{-Br} (1 - e^{-r/D})] . \tag{2.33}$$

This is plotted in Fig. 1 for a typical set of parameters A, B, D.

Pandharipande's differential equation for f is (Pandharipande and Wiringa, 1976; Pandharipande and Bethe, 1973)

$$[-(\hbar^2/M)\nabla^2 + v - \lambda] f = 0 \tag{2.34}$$

with the boundary conditions

$$rf(r) \to 0 \text{ as } r \to 0, f(d) = 1, (df/dr)|_d = 0 . \tag{2.35}$$

Equation (2.34) is used only for $r < d$, and $f(r)$ is put equal to 1 for $r > d$. For a chosen value of d, the value of λ is determined by requiring that, when (2.34) is integrated from $r = 0$ to $r = d$, one finds $df/dr = 0$ at $r = d$. Then d is a variational parameter that can be varied to minimize the energy expectation value. Pandharipande (Pandharipande and Wiringa, 1976; Pandharipande and Bethe, 1973) has given intuitive arguments for this choice of f. Figure 1 shows a plot of the solution of Eq. (2.34) for the potential v_2, which is defined by Eq. (2.47) and plotted in Fig. 7.

As might be expected from the variational principle, the energy expectation value is rather insensitive to the choice of f. For example, consider nuclear matter at $k_F = 1.8$ fm^{-1}, interacting through the central potential v_2. In this case, as we will see in Sec. II.C, the correlation functions B and C of Fig. 1 give practically the same energy expectation value. However, the error in the HNC approximation is much smaller for the Pandharipande correlation function (curve C) than for curve B. This is presumably because of the shorter range of

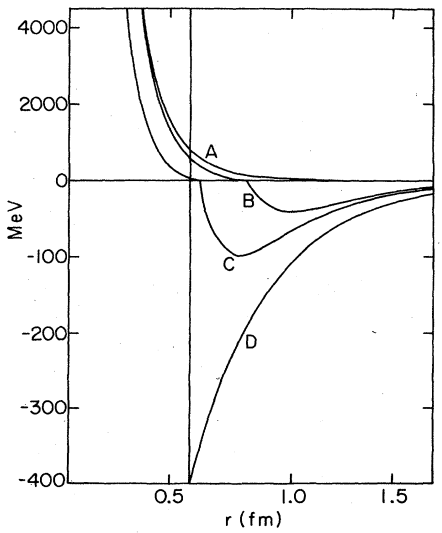

FIG. 7. Typical central potentials. A: "Homework" potential of Eq. (2.45); B: Potential v_2 of Eq. (2.47); C: Potential v_1 of Eq. (2.48); D: Singlet-even component of the OMY potential defined by Eq. (2.49). Note that the energy scale above the horizontal axis is different from that below the axis.

the Pandharipande correlation function. Thus the Pandharipande choice of f is often advantageous, not because it gives a lower energy, but because it permits a more accurate evaluation of the energy expectation value.

C. Fermions with central potentials

In this section we consider variational calculations for fermions interacting through central potentials and give illustrative numerical results from the literature. Most of the ideas developed for bosons in the previous subsection carry over to the fermion case when proper account is taken of antisymmetry.

We devote most of our attention to the Fermi hypernetted-chain (FHNC) method, which gives accurate results over a wide range of densities. But term-by-term summation of the cluster expansion is also of great interest. This is because it is applicable to correlation operators and two-body potentials of arbitrary complexity (Clark and Westhaus, 1968; Clark and Ristig, 1973), while the FHNC method, in its present state of development, is not. A third method for evaluating the energy expectation value is Monte Carlo integration. Such calculations have long been done for bosons, and they have now been extended to fermions with central forces (Ceperley *et al.*, 1977). For central forces, Monte Carlo is probably the best method because the associated error estimates can be made acceptably small and are more reliable than those of other methods. Thus the Monte Carlo results provide the best check on the validity of the other methods. The other methods are of interest because they have been applied to more realistic nuclear potentials, including tensor forces and other complications, while the Monte Carlo method has not. For such potentials, Ristig, Ter Louw, and Clark (1971; 1972) and Kürten and Ristig (1977) have calculated the two- and three-body terms of the cluster expansion, and others (Pandharipande and Wiringa, 1976; Wiringa and Pandharipande, 1978; Rosati, 1977; Smith, 1977; Owen, 1977) are developing partial summation methods analogous to FHNC. However, if the Monte Carlo method could be extended to the full nuclear force, it would probably be better than any method now available.

Still another approach is the lowest-order constrained variational (LOCV) method. The original idea of Pandharipande (1971) was to constrain $h(r)=f^2(r)-1$ to be of such short range that the two-body cluster term alone would accurately approximate the energy expectation value. Later, Pandharipande (Pandharipande *et al.*, 1975) found the method not sufficiently accurate and has given it up in favor of FHNC. The LOCV method has recently been further developed by the Daresbury group (Owen *et al.*, 1976; 1977), who have applied it to many systems, including nuclear matter with the full Reid potential (Owen *et al.*, 1977). They assess the accuracy of the method, however, not by calculating higher-order terms, but by comparison with results of other methods that are supposed to be reliable. The results have recently been criticized on this basis (Kallio and Smith, 1977). So, although the LOCV method may turn out to be useful, it does not at present add to our knowledge of which methods are accurate and which are not.

To apply FHNC, we must require that $f=f(r)$ be a single spherically symmetric function of r with no spin or isospin dependence. This determines the class of two-body potentials that can be treated. In most cases, we will take the potential to be a state-independent function $v(r)$. However, one can also treat a state-dependent potential consisting of four distinct functions of r, one for each of the four possible spin–isospin combinations for a pair of particles. The energy expectation value can be evaluated just as accurately for this case as for a completely state-independent potential. The only question is whether, for a *state-dependent* potential, the energy expectation value calculated with a *state-independent* f is reasonably close to the true ground-state energy. For the OMY potential, as discussed below, this seems to be true. The actual nuclear potential has a more complicated operator structure: Within a given spin–isospin state the potential is a different function of r for different orbital angular momenta L. In this case, regardless of whether a state-independent f gives an adequate wave function, FHNC cannot be used, without making further approximations, to evaluate the energy expectation value. Finally, our restriction of f to a function of r clearly precludes an adequate treatment of strong tensor or spin–orbit forces.

The variational wave function is

$$\Psi = \prod_{i<j}^{A} f(r_{ij})\Phi\,, \tag{2.36}$$

where Φ is a Slater determinant of plane waves with two neutrons and two protons in each momentum state. Just as for bosons, the first step in evaluating the energy expectation value is to calculate the two- and three-body distribution functions $g(r)$ and $g_3(\mathbf{r}_1,\mathbf{r}_2,\mathbf{r}_3)$. We then obtain the expectation value of the potential energy per particle as

$$V = \tfrac{1}{2}\rho \int g(r)v(r)d\tau\,, \tag{2.37}$$

just as for bosons. For bosons, two formulas related by partial integration were available for the kinetic energy. For fermions, three such formulas are in common use. This will be discussed more fully later on. Thus we must calculate $g(r)$ and $g_3(\mathbf{r}_1,\mathbf{r}_2,\mathbf{r}_3)$, and there is a diagram expansion for each of these. The diagrams are more complicated than in the boson case because of the Slater determinant Φ, which was unity in the boson case.

A clear and systematic derivation of fermion diagrams has been given by Gaudin, Gillespie, and Ripka (1971). Here we simply show heuristically how the diagrams of the Bose case must be modified. Equation (2.7) for $g(r)$ contains $\Phi^*\Phi$, and Φ and Φ^* are each a sum of products of plane waves. Suppose we choose a term from Φ containing the factor $\exp(i\mathbf{k}\cdot\mathbf{r}_i)$ and a term from Φ^* containing $\exp(-i\mathbf{k}\cdot\mathbf{r}_j)$, where $\mathbf{k}$ is the momentum of some orbital in the Fermi sea. Then this particular contribution to $\Phi^*\Phi$ will contain the factor $\exp(i\mathbf{k}\cdot\mathbf{r}_{ij})$, where $\mathbf{r}_{ij}=\mathbf{r}_i-\mathbf{r}_j$. Summing over values of $\mathbf{k}$ in the Fermi sea gives

$$(2\pi)^{-3}\int_0^{k_F} d^3k \exp i\mathbf{k}\cdot\mathbf{r}_{ij} = \tfrac{1}{4}\rho l(k_F r_{ij})\,, \tag{2.38}$$

where

$$l(x) = 3x^{-3}(\sin x - x\cos x). \tag{2.39}$$

The presence of this factor is indicated diagrammatically by a dashed line connecting points i and j. So in addition to the dynamical correlation $h(r_{ij}) = f^2(r_{ij}) - 1$, which is represented by a solid line in the diagrams, we now have a statistical correlation $l(k_F r_{ij})$ represented by a dashed line joining points i and j. The dashed lines are called exchange lines. The two-body distribution function $g(r)$ is again given by Eq. (2.9), but a larger class of diagrams contributes to $D(r)$ than in the boson case. The diagrams with no exchange lines are identical to the boson diagrams, but in addition exchange lines may now be drawn in any diagram in such a way that each internal or external point is either (a) untouched by exchange lines, or (b) has exactly one incoming and one outgoing exchange line. Thus the exchange lines always form closed loops. Each internal point *must* be touched by at least one solid line. Only irreducible diagrams are to be included (Fantoni and Rosati, 1974). More precise rules for signs and numerical factors, along with many examples, are given by Pandharipande and Bethe (1973), Fantoni and Rosati (1974), and Zabolitzky (1977). As in the boson case, the Van Kampen cluster expansion is generated by grouping the diagrams according to the number of internal points.

The new element in the diagrams is the exchange line giving the function $l(k_F r)$. This function is unity at $r = 0$ and falls to zero with a range of order k_F^{-1}. However, the average interparticle distance is also of order k_F^{-1}. Thus the range of $l(k_F r)$ is always comparable to the interparticle spacing, and it is therefore not the type of short-range function that is ideal for a cluster expansion. In fact, Brandow (1976) has suggested that antisymmetry of the many-body wave function will cause the cluster expansion to converge too slowly to be useful. His argument is based on an analogy with the Brueckner–Bethe method and runs as follows.

If ϕ_{mn} is the plane wave of relative motion of two particles with momenta m and n in the Fermi sea, then in the Brueckner–Bethe method there occurs a corresponding correlated two-body wave function ψ_{mn}, the first approximation to which is the Bethe–Goldstone wave function (see Sec. III.A). The quantity analogous to ψ_{mn} in the variational method is $f\phi_{mn}$. However, ψ_{mn} is defined so that $\langle \phi_{kl} | \psi_{mn} - \phi_{mn} \rangle = 0$ if either k or l is in the Fermi sea, while $f\phi_{mn}$ will usually not satisfy this condition. Brandow argues that higher terms in the cluster expansion will correct this problem, but that making $f\phi_{mn}$ orthogonal to all momentum states in the Fermi sea will require cluster terms whose order is comparable to the total number of particles. This would imply that summing the cluster series to any reasonable order would be inadequate.

When f is simply a function of r, it is clearly impossible to satisfy Brandow's requirement that $\langle \phi_{kl} | (f-1)\phi_{mn} \rangle = 0$ whenever either k or l is in the Fermi sea. One can, however, choose $f(r)$ to satisfy

$$\overline{\langle \phi_{mn} | (f-1)\phi_{mn} \rangle} = 0, \tag{2.40}$$

where the bar means an average over m, $n < k_F$. This is called the angle-average Pauli condition, and it has long been used in numerical calculations (Bäckman *et al.*, 1972; Chakkalakal *et al.*, 1976). Aside from questions of antisymmetry, this condition is found to be useful in restricting $f(r)$ to the class of functions for which the cluster expansion is likely to be useful (Clark and Ristig, 1972; Chakkalakal *et al.*, 1976).

Brandow has formulated his objection in an intuitive way, and whether or not it is valid is not yet settled. Brueckner (1976) has outlined a formal scheme that may be useful in formulating this question more precisely. His numerical results, however, fail to take proper account of the factor $f^2(r)$ in the two-body distribution function [see Eq. (2.9)] and are therefore spurious. Krotscheck (1976) has given arguments that the cluster expansion should work just as well for fermions as for bosons. There is a need for a more precise understanding of how antisymmetry is treated in the cluster expansion, so that Brandow's objection can be definitely either confirmed or refuted.

In any case, one fact that aids convergence of the cluster expansion is that every internal point in a diagram must be touched by the short-ranged dynamical correlation function $h(r)$. Another aid to convergence is the fact that each exchange line typically carries a numerical factor $\frac{1}{4}$. This is because f is spin and isospin independent, so that a given particle can be exchanged only with that fraction of the other particles having the same spin and isospin. For nuclear matter this fraction is $\frac{1}{4}$.

One can do better than the cluster expansion by using the boson hypernetted-chain partial summation. Recall that the class of fermion diagrams with no exchange lines is identical with the diagrams of the Bose case. Until recently, most calculations applied HNC to these Bose diagrams to obtain a first approximation for the fermion problem. The diagrams with exchange lines were then treated by the perturbation method of Wu and Feenberg (1962).

However, Fantoni and Rosati (1975) have recently shown how to apply the ideas of HNC to the complete set of fermion diagrams, treating the exchange correlations on the same footing as the dynamical correlations. This is a remarkable achievement. The analysis is vastly more complicated than for bosons and leads to a set of four coupled nonlinear integral equations, analogous to the single Eq. (2.23) for bosons. The reader should consult the paper of Fantoni and Rosati (1975) for the derivation and the detailed form of these equations. The reason for expecting the Fermi hypernetted-chain (FHNC) summation to be a good approximation is the same as in the Bose case: The diagrams with the most open structure, such as the chain diagrams, are included in the summation, and only the diagrams with very compact structure, such as the one in Fig. 3, are left out.

A different version of the FHNC summation has been devised by Krotscheck (1975; Krotscheck and Ristig, 1975; Krotscheck, 1977) and applied to neutron and nuclear matter by Krotscheck and Takahashi (1976a; 1976b). It is especially well suited to calculating the long-range behavior of $g(r)$, which in turn determines the low-momentum behavior of the liquid structure function. Which version of FHNC will eventually prove

better for energy calculations remains to be seen. Without attempting to settle this question, we restrict our attention to the Fantoni–Rosati version for two reasons: (1) The Fantoni–Rosati version works very well for the energy, and (2) nearly all calculations done so far have used this version.

We now turn to the crucial question of how accurately one can calculate energy expectation values in the FHNC approximation. We first describe several methods of estimating the error and then illustrate them with numerical calculations.

The first method, suggested by Zabolitzky (1976a), involves comparing different formulas for the kinetic energy. We saw in the boson case that by partial integration one can derive two different formulas for the kinetic energy. For Fermi systems, there are three different formulas for the kinetic energy in common use. The different formulas are denoted by the initials of their inventors, CW for Clark and Westhaus (1966), JF for Jackson and Feenberg (1961), and PB for Pandharipande and Bethe (1973). For bosons, the JF formula requires a knowledge only of the two-body distribution function $g(r)$, *not* of the three-body distribution function g_3. For fermions g_3 occurs in all three formulas for the kinetic energy, although the JF three-body term is numerically very small. Further discussion of these formulas is given by Zabolitzky (1977).

Zabolitzky obtains a second error estimate by evaluating the model kinetic energy $T_{\rm mod}$, defined by

$$T_{\rm mod}=A^{-1}\langle\Phi|T|\Psi\rangle/\langle\Phi|\Psi\rangle\,, \tag{2.41}$$

where Φ is the Fermi-gas wave function and Ψ is the variational wave function of Eq. (2.36). The exact value of $T_{\rm mod}$ is clearly T_ϕ, where

$$T_\phi=0.6\hbar^2k_F^2/2M \tag{2.42}$$

because Φ is an eigenfunction of T with this eigenvalue. But $T_{\rm mod}$ can also be evaluated by applying T to Ψ and obtaining a formula involving the two- and three-body distribution functions, evaluated with $f(r)\to f^{1/2}(r)$ (Zabolitzky, 1976a). Since the function $f^{1/2}(r)$ is very similar to $f(r)$ in shape and range, the FHNC approximation can be applied to $f^{1/2}$ to evaluate $T_{\rm mod}$. The difference between the FHNC result and the exact result T_ϕ is a measure of the error in the FHNC procedure.

A third error estimate is obtained by evaluating correction terms to the FHNC approximation. Just as for bosons, the FHNC approximation is the first term in a systematic expansion. Evaluating the second term, which gives the so-called FHNC/4 approximation, gives an indication of the error in FHNC. Earlier calculations of this type for bosons (Pandharipande, 1973) and fermions (Zabolitzky, 1976a) used the superposition approximation of Eq. (2.29) for $g_3(\mathbf{r}_1,\mathbf{r}_2,\mathbf{r}_3)$, which omits certain terms from the expectation value of the kinetic energy (Smith, 1976; Zabolitzky, 1977). However, a complete FHNC/4 calculation has now been made (Zabolitzky, 1977).

Finally, Monte Carlo integration has recently been applied to the energy expectation value for fermions (Ceperley *et al.*, 1977). The calculations are done by sampling the configuration space of a finite number of particles (typically about 100) in a finite-sized box with periodic boundary conditions. There are two sources of error. One is the statistical error inherent in any Monte Carlo calculation, and the other is caused by using only a finite number of particles. Both errors can be reliably estimated and made acceptably small, e.g., the uncertainty for nuclear matter is 1–2 MeV per nucleon. The Monte Carlo method works at both low and high densities and treats antisymmetry without approximation. Comparison with Monte Carlo results is the most important check on the FHNC results.

We now want to look at illustrative numerical results. It is important to demonstrate that the FHNC method is more widely applicable than low-order truncation of the cluster expansion. For this purpose we need a criterion for applicability of low-order truncation of the cluster expansion. In the Brueckner–Bethe method, this is provided by the value of the parameter κ defined by [see Sec. III.A and Brandow (1966)]

$$\kappa=\rho\int|\phi-\psi|^2d\tau\,, \tag{2.43}$$

where ϕ is a plane wave of relative motion of two particles, and ψ is the correlated two-body wave function. The larger the value of κ, the more important are the many-body correlation terms that are omitted in any practical Brueckner–Bethe calculation. It is intuitively clear that the counterpart to ψ in the variational method is $f\phi$. Substituting $f\phi$ for ψ in Eq. (2.43), and taking proper account of antisymmetry, one gets (Chakkalakal *et al.*, 1976)

$$\kappa_J=\rho\int[f(r)-1]^2[1-\tfrac{1}{4}l^2(k_Fr)]d\tau\,, \tag{2.44}$$

which defines κ_J. For the cluster expansion to succeed, one must have $\kappa_J\ll1$, but we will see that the FHNC approximation is accurate for larger values of κ_J.

The various error estimates are illustrated by the calculations of Zabolitzky (1977) for neutron matter using the "homework potential." This potential is defined (with v in MeV and r in fm by

$$v(r)=9263.1\exp(-4.9r)/r \tag{2.45}$$

and is plotted in Fig. 7. Figure 8 shows the neutron matter results for $\rho=1$ fm^{-3}. This density is six times the empirical saturation density of nuclear matter and, for all cases shown in Fig. 8, we have $\kappa_J>1$. Hence this case provides a very stringent test of the FHNC method.

The Pandharipande correlation function from Eq. (2.34) is used, and the calculations are done for various values of d/r_0, where r_0 is defined by

$$\tfrac{4}{3}\pi r_0^3\rho=1\,. \tag{2.46}$$

For $\rho=1$ fm^{-3} we have $r_0=0.62$ fm. Consider first the FHNC results, which are shown as crosses. For each value of d, three crosses are shown, corresponding to the CW, JF, and PB formulas for the expectation value of the kinetic energy. The expectation value of the potential energy is calculated in exactly the same way in all three methods. For sufficiently small values of d, the three methods give nearly identical results. This suggests that for such short-range correlation functions the terms omitted from the FHNC approximation are

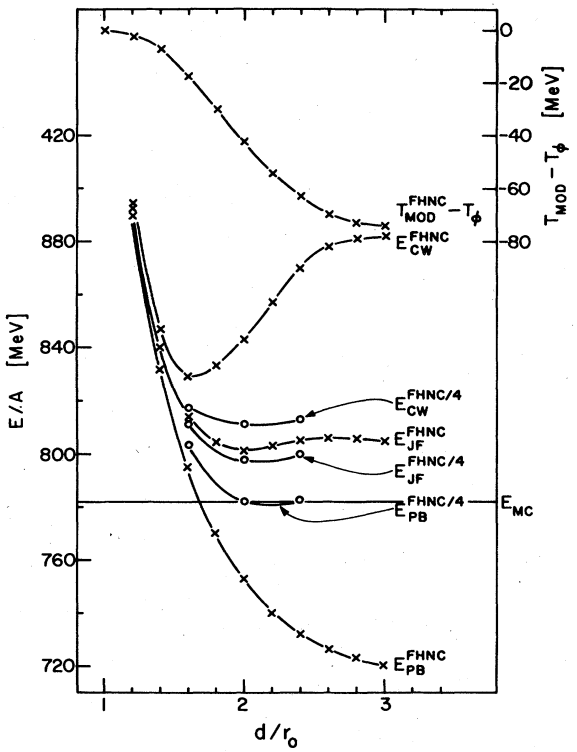

FIG. 8. Calculated values of energy per particle for neutron matter at $\rho = 1.0$ fm^{-3} with the "homework" potential of Eq. (2.45). The results are plotted against the cutoff distance d used in calculating the correlation function from Eq. (2.34). Further discussion is given in the text.

negligible, and the FHNC energy expectation value is very accurate. As d/r_0 is increased from 1.2 to 1.6 two things happen. First, the differences among the CW, JF, and PB energies increase, showing that the terms omitted from FHNC become larger for longer-range correlation functions. Second, the energy expectation value moves down, showing that the variational wave function is improved by using a longer-range correlation function. The difference between the CW and PB energies is a measure of the uncertainty in any one of the three FHNC energies. As d increases beyond $1.6r_0$, this uncertainty rises rapidly, and we cannot tell whether the exact expectation value goes up or down. For any particular value of d, we would estimate the expectation value to be midway between the CW and PB energies, with an uncertainty of about half the difference between these two.

The difference between the FHNC approximation to $T_{\rm mod}$ and the exact value $T_{\rm mod} = T_\phi$ provides our second error estimate and is plotted as the topmost curve in Fig. 8. For all values of d, it is roughly half as large as the difference between the CW and PB energies. Therefore these two error estimates are consistent with each other.

The third error estimate is obtained by calculating the next term in the expansion, i.e., by doing a FHNC/4 calculation. For a given value of d, the three open circles give the FHNC/4 energies calculated with the three different treatments of kinetic energy. For the CW and PB treatments, the change in energy between FHNC and FHNC/4 is comparable to $T_{\rm mod} - T_\phi$. This confirms the two previous error estimates. In this particular case, the change between FHNC and FHNC/4 is much smaller for the JF treatment. However, this is fortuitous—Zabolitzky gives examples where in FHNC the PB treatment is more accurate than JF. The FHNC/4 calculation greatly reduces the spread among the CW, JF, and PB results. This is consistent with the idea that this spread is a measure of the terms neglected in the FHNC approximation.

For d between 2.0 and $2.4r_0$, the expansion starting with FHNC and FHNC/4 seems to be converging to an expectation value in the range 780–820 MeV. We would like to confirm this by comparing with a Monte Carlo calculation of known accuracy. The Monte Carlo result of Ceperley *et al.* (1977) is 782 ± 2 MeV, which is in the expected range. Unfortunately the Monte Carlo calculation used a different form of correlation function and therefore provides no direct evidence on the correct expectation value for the Pandharipande choice of $f(r)$. However, there is substantial evidence (Campani *et al.*, 1976; Fantoni and Rosati, 1976; Zabolitzky, 1977) that the energy expectation value is not very sensitive to the precise form of $f(r)$. (This is what one would expect in a variational method.) So it is extremely probable that the exact expectation value for the Pandharipande choice of f lies in the range spanned by the FHNC/4 results.

We draw two main conclusions from these results. First, FHNC gives accurate results. Second, two easily calculated and reliable error estimates are available in the difference $T_{\rm mod} - T_\phi$ and the spread in the CW, JF, and PB energies. For $d = 2r_0$, for example, from the CW and PB treatments of FHNC, we would estimate the expectation value to be 800 ± 40 MeV, and this is indeed a valid estimate, as shown by the FHNC/4 and Monte Carlo calculations. In most cases, Monte Carlo and FHNC/4 results will not be available, so it is a great advantage that we have two reliable and easily calculated error estimates.

The results of Fig. 8 also illustrate the point that, when minimizing $E_{\rm var}$ with respect to f, it is essential to restrict f to the class of functions for which the approximation used to evaluate $E_{\rm var}$ is accurate. For example, suppose that only the FHNC results, with the PB kinetic energy, were available. We should then be led to the incorrect conclusion that increasing d from 1.6 to $3.0r_0$ substantially reduces $E_{\rm var}$. If we had instead made error estimates, based on the value of $T_{\rm mod} - T_\phi$ and the spread among different treatments of kinetic energy, we would have discovered the rapid rise in uncertainty of the FHNC results as d becomes larger than $2r_0$. Thus these error estimates can save us from drawing wrong conclusions. In fact, without the Monte Carlo and FHNC/4 results, we could not tell from Fig. 8 what the optimum value of d is. However, the situation is much more favorable for central nuclear potentials at densities only one or two times the empirical saturation density of nuclear matter. One typically finds that FHNC remains accurate beyond $d = 2r_0$, but that increasing d beyond $2r_0$ does not lower $E_{\rm var}$.

For further evidence of the validity of FHNC, we turn to the potential v_2, defined by

TABLE I. Summary of FHNC and Monte Carlo results for potential v_2, as discussed in the text.

Corr. fn.	E_{CW}	E_{PB}	E_{est}	$T_{mod}-T_{\phi}$	E_{MC}
MC	12.4	2.1	7.2±5.2	5.0	3.4±1.5
P($d=2r_0$)	8.0	3.4	5.7±2.3	1.7	

$$v_2(r) = -10.463e^{-x}/x + 105.468e^{-2x}/x - 3187.8e^{-4x}/x + 9924.3e^{-6x}/x, \quad (2.47)$$

where $x=0.7r$, r is in fm, and v_2 is in MeV. This potential is plotted in Fig. 7. Some of Zabolitzky's (1977) FHNC results for nuclear matter with this potential are shown in Table I. The results in the first row are for $\rho=0.386$ fm^3, and in the second row for $\rho=0.394$ fm^{-3} ($k_F=1.8$ fm^{-1}). This difference in density is negligible for the present discussion. The lowest-order approximation to the Brueckner–Bethe parameter κ is 0.27, so that this is a reasonably difficult case.

The first row is for the correlation function of Eq. (2.33), which is plotted as curve B in Fig. 1 and has been used in Monte Carlo calculations (Ceperley *et al.*, 1977). We refer to this correlation function as the Monte Carlo (MC) correlation function. The second row shows results for the Pandharipande correlation function with $d=2r_0$, which is plotted as curve C in Fig. 1. In each case the estimated FHNC energy E_{est} is taken to be midway between E_{CW} and E_{PB} with an uncertainty of $\frac{1}{2}(E_{CW}-E_{PB})$. This error estimate is seen to be close to $T_{mod}-T_{\phi}$. For the MC correlation function, the Monte Carlo result of Ceperley, Chester, and Kalos (1977) is shown. (This paper quotes a statistical error of 5.0 MeV. However, Dr. Kalos has informed me that the correct statistical error is 1.0 MeV. From other results in the paper, it appears that finite-size effects raise the total uncertainty in the MC result to 1.5 MeV, and this uncertainty is shown in Table I.) Comparison with the Monte Carlo result shows that the FHNC estimate for the expectation value is correct within the estimated error. The Pandharipande correlation function is of shorter range than the Monte Carlo one, and this leads to a smaller error in the FHNC estimate. But the energy is not significantly different from that obtained with the longer-range MC correlation function. This illustrates the insensitivity of the energy to the choice of f. For the MC correlation function, the exact expectation value lies near the lower end of the FHNC estimate. This behavior is observed in other cases as well, so that the best estimate for the expectation value, on the basis of FHNC calculations alone, is usually between E_{PB} and $\frac{1}{2}(E_{CW}+E_{PB})$. However, the main conclusion to be drawn from Table I is that the FHNC estimate of the expectation value, and the associated error estimate, are both reliable.

Having established the reliability of the FHNC approximation, we look at additional results for central potentials. Figure 9 shows results for v_2, using the Pandharipande correlation function with $d=2r_0$ (Zabolitzky, 1977; Benhar *et al.*, 1976). The upper limit of the FHNC band is given by $\frac{1}{2}(E_{CW}+E_{PB})$ and the lower limit by E_{PB}, in accord with the discussion in the last paragraph. Also shown is the lowest-order Brueckner–Bethe calculation (Pandharipande *et al.*, 1975). It is seen to lie definitely above the FHNC upper bound. This discrepancy is typical and will be discussed later.

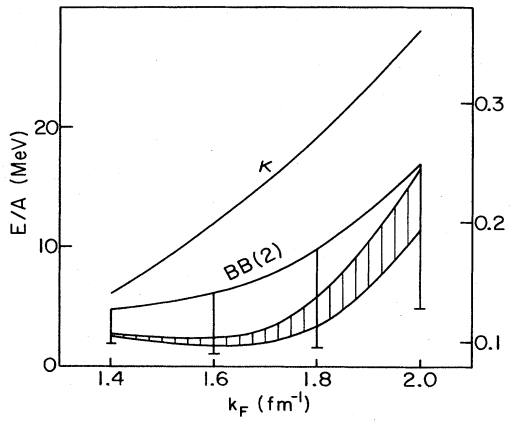

FIG. 9. Calculated energy per particle of nuclear matter plotted against Fermi momentum k_F for the potential v_2 of Eq. (2.47). The shaded region shows the FHNC result with the error estimate discussed in the text. The curve labeled BB(2) gives the lowest-order Brueckner–Bethe result calculated with a single-particle spectrum given by pure kinetic energy above the Fermi sea. The error bars extending downward from this curve have magnitude κD_2 and determine the expected order of magnitude of higher-order corrections to the Brueckner–Bethe result. The lowest-order approximation to the Brueckner–Bethe parameter κ is also plotted, using the right-hand vertical scale.

We note here that the earliest variational calculation with potential v_2 (Pandharipande *et al.*, 1975) did not include a full FHNC calculation and gave more binding energy than the results shown in Fig. 9. The latter results should be more accurate because they are obtained from a complete FHNC calculation and are confirmed by Monte Carlo results.

A similar plot is shown in Fig. 10 for the potential v_1, which is given by

$$v_1(r) = -10.463e^{-x}/x - 1650.6e^{-4x}/x + 6484.2e^{-7x}/x, \quad (2.48)$$

where $x=0.7r$, v is in MeV, and r in fm. This potential is plotted in Fig. 7. The lowest-order approximation to κ is always less than 0.1 for v_1, and the uncertainty in the FHNC estimate of the expectation value is only about

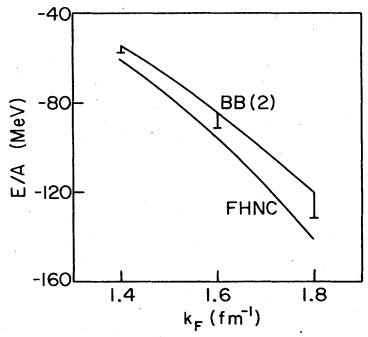

FIG. 10. Same as Fig. 9 for the potential v_1 of Eq. (2.48).

0.1 MeV, too small to be shown on the graph. Again, the lowest-order Brueckner–Bethe result lies substantially higher.

The first calculations showing a large discrepancy between lowest-order Brueckner–Bethe results and the variational method were done by Bäckman, Chakkalakal, and Clark (1969). They did not use FHNC but calculated the two- and three-body terms in the cluster expansion for the expectation value. Since FHNC calculations have now been done for the same potential, the cluster expansion can be tested. This is important because the cluster expansion, calculated through three-body terms, has been applied to tensor forces: It is clearly of great interest to know whether it is accurate for the simpler case of central forces.

The calculations have been done for the OMY (Ohmura, Morita, and Yamada, 1956) and IY (Iwamoto and Yamada, 1957) potentials, and we show results for the OMY potential. This potential has a hard core of radius $c = 0.6$ fm. Outside the core, the potential is zero in odd states, i.e., spin–isospin states with $(S, T) = (0, 0)$ or $(1, 1)$. For the other two (S, T) combinations, the extra-core OMY interaction is given by

$$v = -397.31 \exp[-2.627(r - c)], r > c, (S, T) = (0, 1), \tag{2.49}$$

$$v = -947.02 \exp[-3.677(r - c)], r > c, (S, T) = (1, 0), \tag{2.50}$$

where v is in MeV and r and c are in fm. The singlet-even $(S, T = 0, 1)$ component is plotted in Fig. 7. Because of the large core radius κ_J is fairly large (0.3 at the saturation density) and provides a demanding test of the cluster expansion.

We show results obtained with the three-parameter correlation function (Bäckman *et al.*, 1969) used in the original work (Bäckman *et al.*, 1972). This allows comparison with a FHNC calculation (Campani *et al.*, 1976) that used the same correlation function and the JF treatment of kinetic energy. However, the simpler correlation function of Eq. (2.32) has been found to give nearly the same results (Chakkalakal *et al.*, 1976). The results are plotted in Fig. 11, where the FHNC and cluster calculation results are labeled FHNC and CL, respectively. The values of κ are taken from the Brueckner–Bethe calculation (Bäckman *et al.*, 1972), but they are nearly the same as the values of κ_J. For all densities up to $k_F = 1.6$ fm^{-1}, the contribution from the three-body cluster term is less than 3 MeV, remarkably small for values of κ as large as 0.3. Since κ is about the same as for the potential v_2, the accuracy of the FHNC expectation value can be expected to be 1–3 MeV. It would be desirable to verify this by applying one or more of the error estimates mentioned above.

The FHNC and cluster calculations agree to within about 1 MeV. We conclude that the cluster expansion is very probably accurate to 2–3 MeV for this case. The lowest-order Brueckner–Bethe calculation (Bäckman *et al.*, 1972) lies much higher. The success of the cluster expansion in this case makes it reasonable to apply the same method to tensor forces. Work has begun in this direction and will be discussed in the next subsection.

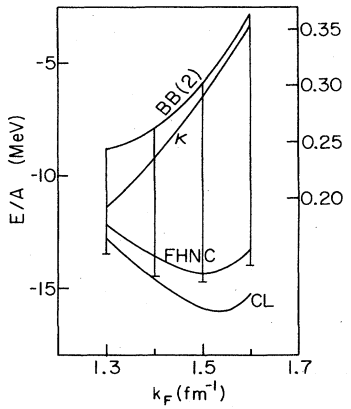

FIG. 11. Calculated energy per particle of nuclear matter for the OMY potential. The curves labeled FHNC and CL are variational calculations and are described in the text. The Brueckner–Bethe results labeled BB(2) and κ have the same significance as in Fig. 9.

We have so far considered only the question of how accurately the expectation value can be calculated. The other interesting question is, how close is the expectation value to the exact ground-state energy? We now review the available evidence on this point.

The most direct information comes from the work of Clark *et al.* (1975) using the OMY potential. One can develop a perturbation formalism that starts with the variational wave function as unperturbed wave function. Evaluating the perturbation series would eventually generate the exact Ψ and E from the variational Ψ and E. The leading perturbation correction to the energy can itself be expanded in a cluster series, and Clark *et al.* (1975) have evaluated the two-body term in this expansion. For the OMY potential, they find the binding energy is increased by 4–5 MeV, nearly independent of density. Part of this correction accounts for the fact that the OMY potential is state dependent, while the correlation function used is not. Putting the triplet-even interaction equal to the singlet-even interaction in the OMY potential [the resulting interaction is called the IY potential (Iwamoto and Yamada, 1957)] reduces the perturbation correction to 2.0–2.5 MeV. The IY potential is still state dependent because it has no attractive force in odd states, and part of the perturbation correction is presumably due to this fact. Hence, for state-independent potentials such as v_1 and v_2, the expectation value with the variational wave function of Eq. (2.36) could well be within 2 MeV of the true ground-state energy.

For Bose systems, precise information is available on this point because Kalos (1970, 1974) has developed a Monte Carlo method to calculate the *exact* ground-state energy. In this "Green's-function Monte Carlo method" uncertainties due to statistics and finite-size effects can be made very small. A system of interacting bosons has been treated in this way (Ceperley *et al.*, 1976), using the Yukawa-core potential

$$v(r) = 5725 \exp(-4.1r)/r, \tag{2.51}$$

where v is in MeV and r in fm. It was found that the expectation value in the trial wave function (2.6) is within

1% of the exact ground-state energy for densities up to 50 times the empirical saturation density of nuclear matter. Kalos (1977) has made a similar comparison for the Bose system liquid ^{4}He, using the Lennard-Jones potential, which has a strong short-range repulsion behaving as r^{-12}. Near the saturation density of liquid ^{4}He he finds the exact ground-state energy to lie 15% below the variational result obtained with the wave function (2.6). Thus the variational upper bounds with the usual choice of wave function are very close to the exact ground-state energies for potentials with Yukawa cores, and moderately close for potentials with more singular cores. The estimate of 2 MeV in nuclear matter, obtained in the preceding paragraph, was for a potential with an infinitely repulsive core. Hence we may expect even better accuracy for potentials with Yukawa-shaped cores.

Further indication that the variational energy is very close to the exact ground-state energy comes from evaluating the model energy defined by

$$E_{\rm mod}=A^{-1}\langle\Phi|H|\Psi\rangle/\langle\Phi|\Psi\rangle\,, \tag{2.52}$$

where Ψ is the variational wave function and Φ is the free Fermi-gas wave function. This was suggested by Kümmel (1976) and has been carried out by Zabolitzky (1976a) using FHNC to evaluate $E_{\rm mod}$. If Ψ were an eigenstate of H, then $E_{\rm mod}$ would agree with the energy expectation value $E_{\rm var}$. Thus a necessary condition for Ψ to accurately approximate the true ground-state wave function is that $E_{\rm mod}$ be close to $E_{\rm var}$. Unfortunately, it is hard to make this statement quantitatively useful. For a known difference between $E_{\rm mod}$ and $E_{\rm var}$, there seems to exist no quantitative estimate of the difference between $E_{\rm var}$ and the exact ground-state energy. Also, even exact agreement between $E_{\rm mod}$ and $E_{\rm var}$, although suggestive, does not prove anything. The agreement could conceivably be purely accidental.

Nevertheless, the numerical results are remarkable. For the potentials v_1 and v_2, at all densities up to twice the empirical density of nuclear matter, $E_{\rm mod}$ agrees with $E_{\rm var}$ to 1 MeV or better (Zabolitzky, 1976a). These results use the Pandharipande correlation function with $d=2r_0$. Since this close agreement holds over a range of densities for two quite different potentials, it is unlikely to be accidental. The results are consistent with $E_{\rm var}$ being very close to the exact ground-state energy.

Let us summarize the main results of this subsection. For central forces, the FHNC approximation for the energy expectation value is accurate up to densities at least twice the empirical saturation density of nuclear matter. Approximate evaluation of the model kinetic energy, and the spread among various treatments of the expectation value of the kinetic energy, provide two reliable and easily calculated error estimates for the FHNC result. Since no calculation is useful without an error estimate, it is important to compute these error estimates in practical calculations.

Term-by-term summation of the cluster expansion has not been as carefully tested as FHNC. In the one case studied, the two- and three-body cluster terms gave an accurate expectation value in spite of a fairly large value of 0.3 for the expansion parameter κ_f. Thus the extension of this technique to tensor forces (discussed in the next subsection) is reasonable.

For state-independent central forces, it is probable that the energy expectation value obtained with the wave function of Eq. (2.36) is within 2 MeV of the exact ground-state energy.

The outstanding feature of variational calculations with central forces is that the error estimates are highly reliable. This is largely because Monte Carlo calculations have been done. This situation contrasts sharply with that of variational calculations with tensor forces and with that of Brueckner–Bethe calculations with any potential. In the latter two cases, the best one can hope for at present is a physically plausible expansion in which the first two or three terms behave well. Therefore, variational calculations with central forces can confidently be used as a standard against which Brueckner–Bethe calculations are to be tested. The lowest-order Brueckner–Bethe results lie consistently above the variational upper bounds. So it is of great interest to see whether higher-order terms in the Brueckner–Bethe method will repair this discrepancy.

D. Fermions with realistic forces

In this subsection we consider variational calculations for interactions with tensor forces and the other complexities present in phenomenological nuclear forces. In this case the two-body correlation operator f must be more general than multiplication by a function $f(r)$. One part of f will consist of multiplication by a function of r (this will be called the state-independent part), and the other part will contain more complicated operators such as spin, isospin, the tensor operator, etc. (this will be called the state-dependent or operator part). Neither the Monte Carlo method nor the FHNC approximation has yet been formulated for the case when f has a nonzero operator part. As a result, the reliability of the calculations is much less certain than for central forces.

Two approaches have been used so far. The first, which has been used by the Clark–Ristig group (Ristig *et al.*, 1971; 1972; Kürten and Ristig, 1977) is to evaluate the two- and three-body terms in the Van Kampen cluster expansion (Van Kampen, 1961; Clark and Westhaus, 1968; Clark and Ristig, 1973). In the second approach, which was begun by Pandharipande and Wiringa (1976; Wiringa and Pandharipande, 1978) and is now also being pursued by several other groups (Rosati, 1977; Smith, 1977; Owen, 1977), FHNC is applied to the state-independent part of f. Then, in analogy with the FHNC method, one tries to identify and sum the most important terms that involve the operator part of f. The calculations in both methods are inevitably complicated, and at present there are no firm estimates of the errors.

The Van Kampen cluster expansion (Van Kampen, 1961) can be worked out order by order for arbitrarily complicated correlation operators and interactions (Clark and Westhaus, 1968; Clark and Ristig, 1973). Ristig, Ter Louw, and Clark (1971, 1972) have given explicit formulas for the two- and three-body terms, using the CW treatment of kinetic energy. Numerical results have been obtained by them and also by Kürten

and Ristig (1977). They both used the Gammel–Christian–Thaler (1957) potential, which we denote GCT, and potentials 5200 and 5100 of Gammel and Thaler (1960). These potentials all have an infinitely repulsive core of radius 0.5 fm. The extra-core interaction is given by a single Yukawa function that is different for singlet-even, triplet-even, singlet-odd, and triplet-odd states. In addition, there is a tensor force in the triplet states. All three potentials are fitted to low-energy scattering data and to the properties of the deuteron. Potentials with no spin–orbit force were selected on purpose in order to study tensor effects without other complications.

The two-body correlation operator is taken to be

$$F_2 = f(r_{12})[1 + q(r_{12})t_{12}], \tag{2.53}$$

where f and q are spherically symmetric functions of r_{12}, and t_{12} is independent of $|\mathbf{r}_{12}|$ and contains the tensor operator and a projection operator onto triplet-even states. The three-body correlation operator is taken to be

$$F_3 = f(r_{12})f(r_{13})f(r_{23})[1 + q(r_{12})t_{12} + q(r_{13})t_{13} + q(r_{23})t_{23}], \tag{2.54}$$

which is consistent with the cluster requirement (2.5). Note that this is simpler than the symmetrized product of two-body correlation operators.

A cutoff parameter d is used as a variational parameter. For a given value of d, $f(r)$ and $q(r)$ are determined by minimizing the two-body cluster energy, subject to the conditions that: (i) $f(r)$ and $q(r)$ go smoothly to 1 and 0, respectively, as $r \to d$, so that $f(r) = 1$ and $q(r) = 0$ for $r > d$; (ii) $f(r)$ satisfies the angle-average Pauli condition (2.40). Once $f(r)$ and $q(r)$ are determined, the two- and three-body cluster terms for the energy are evaluated. Minimizing their sum then determines d. The resulting values of d for the GCT, 5200, and 5100 potentials are, respectively 2.2, 2.5, and 2.9 fm, and are nearly independent of density.

The results are shown in Fig. 12. The results for the 5200 potential have been published (Kürten and Ristig, 1977), and those for the GCT and 5100 potentials were kindly supplied by Dr. Ristig. For none of the potentials does the variational result saturate below $k_F = 1.7$ fm^{-1}. The calculated saturation properties are correlated with the strength of the tensor force: The GCT potential has the weakest tensor force, and the 5100 potential, which comes closest to saturating, has the strongest tensor force.

The values of the three-body cluster term and of the expansion parameter κ_J, which now includes tensor contributions, are plotted for the GCT potential. Both are similar in size to their values for the OMY central potential, for which the cluster expansion was found to be accurate. Since tensor correlations are qualitatively different from central correlations, this does not prove the accuracy of the calculations, but there is no indication of anything wrong. A rough estimate of the error caused by omission of higher-order terms is κ_J^2 times the two-body cluster term. Error bars of this size are shown in Fig. 12 for the GCT potential.

To pin down the error more accurately, an estimate

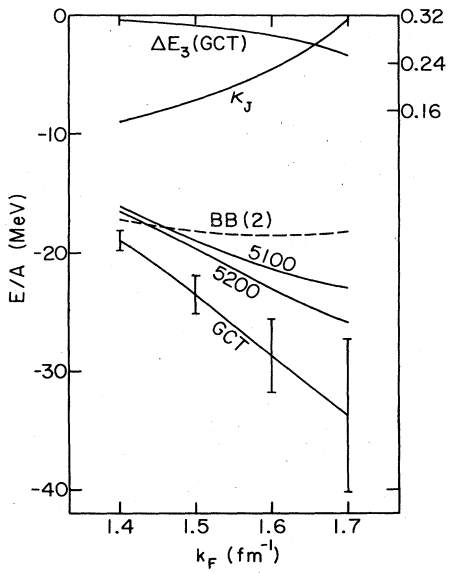

FIG. 12. Calculated energy per particle of nuclear matter, with interactions containing tensor forces, plotted against Fermi momentum k_F. The meanings of the various curves are described in the text.

of the four-body cluster term would be helpful. The spread among different treatments of the kinetic energy might also be useful in this regard. The CW treatment was used to obtain the results in Fig. 12, but the PB and JF formulas could also be applied, and a comparison of the results would give an idea of the error.

The results of a two-body Brueckner–Bethe calculation (Brueckner and Gammel, 1958) are shown for the GCT potential. Error bars are not shown because the required values of κ are not available. However, if these values of κ are comparable to the corresponding values of κ_J, the higher-order terms in the Brueckner–Bethe calculation could account for the discrepancy with the variational result.

Let us now turn to the work of Pandharipande and Wiringa (PW). Instead of calculating successive terms in the cluster expansion, they attempt to identify the most important higher-order terms and to sum them using integral equations, in analogy to the FHNC approximation for state-independent correlation functions. This is not an easy task. The analog of the expansion in irreducible diagrams, which is valid for state-independent correlation functions, is immensely more complicated for correlation functions that contain operators. The method is being actively developed by several groups (Wiringa and Pandharipande, 1978; Rosati, 1977; Smith, 1977; Owen, 1977), and we merely give the basic ideas and describe the present results.

Let us first assume that the two-body potential v has six components: four independent central components in the singlet-even (SE), singlet-odd (SO), triplet-even (TE), and triplet-odd (TO) states, and two independent tensor components in the TE and TO states. Any such potential can be written in the form

$$v_{12} = \sum_{i=1}^{6} v^i(r_{12})O^i \tag{2.55}$$

where the v^i are functions of r_{12}, and the O^i, $i=1,2,\ldots,6$ are, respectively, the operators 1, $\sigma_1\cdot\sigma_2$, $\tau_1\cdot\tau_2$, $(\sigma_1\cdot\sigma_2)(\tau_1\cdot\tau_2)$, S_{12}, and $\tau_1\cdot\tau_2 S_{12}$, where S_{12} is the tensor operator. This form of v_{12} neglects two essential features of actual nuclear forces—the spin-orbit, or $\mathbf{l}\cdot\mathbf{S}$, interaction and the difference between the SE interaction in $^1S_0$ and $^1D_2$ waves. These will be considered later.

The correlation function is written similarly as

$$f_{12}=\sum_{i=1}^{6} f^i(r_{12})O^i . \tag{2.56}$$

At $r=d$, the six functions $f^i(r)$ are required to go smoothly to either unity (for $i=1$) or zero (for $i\neq 1$). The range d is treated as a variational parameter. The six independent functions $f^i(r)$ are obtained by solving the Pandharipande differential equation (2.34) in various partial waves. The uncoupled $^1S_0$ and $^1P_1$ states provide the SE and SO correlation functions. In the coupled $^3S_1-^3D_1$ channel, Eq. (2.34) reduces to two coupled differential equations whose solutions give both a central and a tensor correlation function for TE states. Similarly, the $^3P_2-^3F_2$ channel provides central and tensor correlation functions for the TO states. This gives six independent functions of r, and the six functions $f^i(r)$ are linear combinations of these. It turns out that $|f^i(r)|\ll 1$ for all $i\neq 1$, and this fact is used in the approximation scheme.

In calculating the expectation value of v_{12}, one encounters the expression $f_{12}v_{12}f_{12}$, which comes from $\Psi^* v_{12}\Psi$. This is combined with that part of the kinetic energy containing $\nabla_{12}^2 f_{12}$ to get $f_{12}[-(\hbar^2/M)\nabla_{12}^2+v_{12}]f_{12}$. For $r_{12}<d$, one can use Eq. (2.34) (suitably generalized to include tensor coupling and with different constants λ in different partial waves) to express this in terms of products of the constants λ and the $f^i(r_{12})$. For $r_{12}>d$, we have simply v_{12}. In either case, using Eqs. (2.55) and (2.56) for v_{12} and f_{12}, one can write

$$f_{12}[-(\hbar^2/M)\nabla_{12}^2+v_{12}]f_{12}=\sum_{i=1}^{6} V^i(r_{12})O^i \tag{2.57}$$

for appropriate functions $V^i(r_{12})$. In deriving this result, one uses the following very convenient property of the six operators O^i: The product of any two is a linear combination of the original six operators. This property would not hold if $\mathbf{l}\cdot\mathbf{S}$ were included in the O^i. For this reason the operator $\mathbf{l}\cdot\mathbf{S}$ is troublesome. Explicit formulas for the effective potentials $V^i(r_{12})$ are given by Pandharipande and Wiringa (1976).

The potential energy and most of the kinetic energy are to be obtained by combining Eq. (2.57) with the passive f_{ij} (a passive f_{ij} is one for which the pair ij differs from 12, such as f_{13}) and integrating. Since $|f^{i\neq 1}(r)|\ll 1$, the first approximation is to set all passive $f^{i\neq 1}$ equal to zero and apply FHNC to the passive $f^{i=1}$. Terms in the kinetic energy not accounted for in Eq. (2.57) are calculated using FHNC with the PB treatment of kinetic energy. Also, some terms are added to Eq. (2.57) so that the $\mathbf{l}\cdot\mathbf{S}$ interaction and the difference between $^1S_0$ and $^1D_2$ interactions are treated correctly in the two-body cluster term but only approximately in the higher FHNC terms.

To go beyond this approximation, we must consider terms with passive $f^{i\neq 1}$. Motivated by the fact that $|f^{i\neq 1}|\ll 1$, PW in their earlier work (Pandharipande and Wiringa, 1976) included terms up to second order in passive $f^{i\neq 1}$. This procedure is different from term-by-term summation of the cluster expansion. The three-body cluster term contains terms up to fourth order in passive $f^{i\neq 1}$. Including only terms up to second order omits part of the three-body term but sums many terms involving more than three particles. The PW method also differs from the cluster expansion by including a full FHNC calculation for terms of zero order in passive $f^{i\neq 1}$.

For $d=2r_0$ [see Eq. (2.46)] PW found that the Reid potential saturates in this approximation at $\epsilon=-25$ MeV, $k_F=1.7$ fm^{-1}, very far from the empirical saturation point ($\epsilon=-16\pm 1$ MeV, $k_F=1.29$–1.44 fm^{-1}). However, they also found that increasing d causes the calculated energy expectation value to decrease rapidly without limit. This is not entirely unexpected. Even though the passive $f^{i\neq 1}$ are small compared to 1, their effect must eventually become large when their range d becomes sufficiently large. Thus the approximation of evaluating the energy expectation value to second order in the passive $f^{i\neq 1}$ must break down for large enough d.

When the correlation operator is a spherically symmetric function of r, the solution to this problem was found in the preceding subsection to be the summation of chain diagrams, leading eventually to the FHNC approximation. In their recent work (Wiringa, 1978), PW have summed many additional diagrams involving passive $f^{i\neq 1}$. As a result, they find the dependence of the energy on d to be much improved. The calculated energy expectation value still decreases with d, but much more slowly than before, and this result is encouraging. For the potential of Reid (1968) at $k_F=1.8$ fm^{-1}, increasing d from 2.1 to 2.7 fm causes the calculated expectation value to change from -16.2 to -21.1 MeV per particle. PW also find somewhat less binding energy than before. Some of the results (Wiringa and Pandharipande, 1978) are plotted in Fig. 13 as curves PW1 and PW2. These results are obtained using a

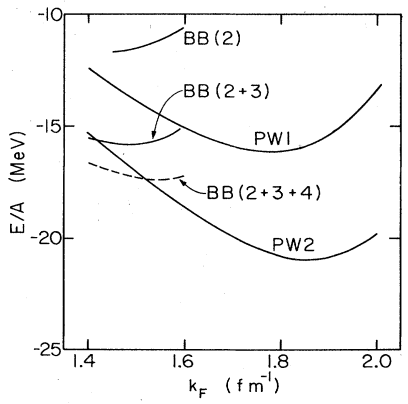

FIG. 13. Calculated values of the energy per particle of nuclear matter plotted against Fermi momentum for the Reid potential. Curves PW1 and PW2 are variational calculations by Pandharipande and Wiringa, described in Sec. II.D. The other curves are obtained from the Brueckner–Bethe method and are described in Sec. III.B.

slightly simplified method in which the calculated energy *does* have a minimum in d. [This method nevertheless goes far beyond the one used (Pandharipande and Wiringa, 1976) by PW in their earlier work.] In all cases shown, the value of d that minimizes the energy is found to lie in the range 2.3–2.7 fm. The lower curve PW2 differs from the upper curve PW1 by allowing the correlation operator f used in the two-body cluster term to depend on the relative momentum of the two interacting particles. The higher-order terms are the same for the two curves. Although the two curves differ by several MeV in energy, they agree in predicting that the Reid potential saturates near $k_F = 1.8$ fm^{-1}, far above the empirical range of 1.29–1.44 fm^{-1}. Thus, PW still conclude that the Reid potential predicts disastrously wrong saturation properties for nuclear matter. A comparison of these results with the Brueckner–Bethe results will be made in Sec. III.

We do not yet have a good quantitative estimate of the error in the PW evaluation of the energy expectation value. We expect that, as the density is increased or as the range d of the correlation function is increased, a point will be reached where complicated many-body correlations that are not included in the calculation will become important, and the PW approximation will break down. But at present there is no clear indication of when this point is reached. A useful error estimate could also be obtained by calculating the spread among the kinetic energies obtained using the PB, JF, and CW methods. This was found to give a reliable error estimate for central forces. The difference $T_{\rm mod} - T_\phi$, which also gives a reliable error estimate for central forces, may be less useful as a test of tensor correlations. In the numerator $\langle\Phi|T|\Psi\rangle$ of Eq. (2.41) for $T_{\rm mod}$, for example, tensor correlations contribute nothing to the dominant two-body cluster term. Even so, it would be worthwhile to verify that $T_{\rm mod} - T_\phi$ is small as a consistency check.

In summary, both variational approaches for tensor forces have a reasonable chance for success. Additional work, possibly along the lines suggested above, is required in both methods in order to obtain more reliable error estimates. It would also be interesting to apply both methods to the same two-body potential and compare the results.

III. THE BRUECKNER-BETHE METHOD

A. Description of the method

In this subsection we describe the Brueckner–Bethe method as presently practiced, and in the following subsection we discuss tests of the validity of this method.

In the Brueckner–Bethe method one represents the many-body ground state Ψ in the form

$$\Psi = \left(1 + \sum_{n\geq 2} F_n\right)\Phi , \tag{3.1}$$

where Φ is the free Fermi-gas state, and the operator F_n excites exactly n particles out of the Fermi sea. If Ψ satisfies the Schrödinger equation

$$H\Psi = E\Psi , \tag{3.2}$$

then it follows for a Hamiltonian of the form (1.1) that

$$E = \langle\Phi|T|\Phi\rangle + \langle\Phi|V + VF_2|\Phi\rangle , \tag{3.3}$$

where

$$T = \sum_{i=1}^{A} T_i , \quad V = \sum_{i<j}^{A} v_{ij} . \tag{3.4}$$

Note that only F_2 appears in the exact formula (3.3) for the energy.

The energy per particle ϵ is then exactly

$$\epsilon = \tfrac{3}{5}\hbar^2 k_F^2/2M + \tfrac{1}{2}A^{-1}\sum_{m,n<k_F}\langle\phi_{mn}|v|\psi_{mn}\rangle , \tag{3.5}$$

where ϕ_{mn} is the plane wave of relative motion for two particles with momenta $\mathbf{m}$ and $\mathbf{n}$, and the nuclear matter two-body wave function ψ_{mn} is defined by

$$\begin{aligned}\psi_{mn}(\mathbf{r}_1,\mathbf{r}_2) &= \langle\Phi|a_m^\dagger a_n^\dagger a(\mathbf{r}_1)a(\mathbf{r}_2)|\Psi\rangle \\ &= \phi_{mn}(\mathbf{r}_1,\mathbf{r}_2) + \langle\Phi|a_m^\dagger a_n^\dagger a(\mathbf{r}_1)a(\mathbf{r}_2)F_2|\Psi\rangle ,\end{aligned} \tag{3.6}$$

where $a_m^\dagger$ creates a nucleon of momentum $\mathbf{m}$, and $a(\mathbf{r})$ destroys a nucleon at the point $\mathbf{r}$.

The most widely used procedure for obtaining approximate solutions of Eq. (3.2) amounts to expanding the operator F_n and the energy E into formal perturbation series that are then selectively summed. The first step is to introduce a single-particle potential

$$U = \sum_{i=1}^{A} U_i \tag{3.7}$$

by writing

$$H = H_0 + H_1 , \tag{3.8}$$

$$H_0 = T + U , \tag{3.9}$$

$$H_1 = V - U . \tag{3.10}$$

We assume the system to be translationally invariant so that $U = U(k)$ is diagonal in momentum space. There is some evidence that at very high density ($k_F \geq 2.2$ fm^{-1}, compared to the empirical saturation value $k_F \cong 1.36$ fm^{-1}) a lower energy is obtained using a wave function having spatial density oscillations (Calogero and Palumbo, 1973). We are interested in much lower densities and therefore assume translational invariance.

The perturbation series in powers of H_1 can be generated by iterating the equations

$$E = E_0 + \langle\Phi|(H_1 + H_1F_2)|\Phi\rangle , \tag{3.11}$$

$$F = 1 + (1 - |\Phi\rangle\langle\Phi|)(E - H_0)^{-1}H_1F , \tag{3.12}$$

where

$$F = 1 + \sum_{n\geq 2} F_n , \tag{3.13}$$

$$H_0\Phi = E_0\Phi . \tag{3.14}$$

The terms in the perturbation series are conveniently represented by Goldstone diagrams (Goldstone, 1957). All unlinked diagrams cancel in the series for E and F_2, but F_n contains terms represented by unlinked as well as linked diagrams. If we define S_n to be the linked part of F_n, then it can be shown that $S \equiv \sum_{n\geq 2} S_n$ is related to F by (Coester, 1958)

$$F = \exp(S) . \tag{3.15}$$

The coupled nonlinear equations for the S_n that follow

from Eq. (3.2) provide a flexible starting point for different approximation schemes that need not involve formal infinite expansion followed by selective resummation (Coester, 1969; Kümmel *et al.*, 1978). These equations have been called the exp(S) equations (Kümmel *et al.*, 1978).

However, all presently available calculations for nuclear matter can be described in the more familiar language of sums of classes of Goldstone diagrams (Day, 1967; Bethe, 1971; Sprung, 1972; Köhler, 1975), which we will use for the following discussion. We first describe the hole–line expansion with the conventional single-particle spectrum in some detail. The other approximations of present interest can then be described as modifications of the hole–line expansion.

Let $\psi_{mn}^{(h)}$ be the contribution to the two-body wave function from diagrams with h independent hole lines, except that $\psi_{mn}^{(2)}$ also includes the uncorrelated two-body wave function ϕ_{mn}. By a hole line is meant any line labeled by a momentum smaller than k_F. The number of *independent* hole lines in a diagram is the number of momenta smaller than k_F that can be independently specified, after all restrictions due to momentum conservation are taken into account (examples will be given below). Then we can write

$$\psi_{mn} = \sum_{h\geq 2} \psi_{mn}^{(h)} , \tag{3.16}$$

and putting this into Eq. (3.5) gives the hole–line expansion for the energy per particle as

$$\epsilon = \tfrac{3}{5}\hbar^2 k_F^2/2M + \sum_{h=2}^{\infty} D_h , \tag{3.17}$$

where

$$D_h = \tfrac{1}{2}A^{-1} \sum_{m,n<k_F} \langle \phi_{mn} | v | \psi_{mn}^{(h)} \rangle . \tag{3.18}$$

The lowest-order (two-hole–line) approximation $\psi_{mn}^{(2)}$ is given by the solution of the Bethe–Goldstone equation

$$\begin{aligned} \psi_{mn}^{(2)} &= \phi_{mn} - (Q/e)v\psi_{mn}^{(2)} , \\ &= \phi_{mn} - (Q/e)G\phi_{mn} , \end{aligned} \tag{3.19}$$

where the reaction matrix G is the solution of the equation

$$G = v - v(Q/e)G . \tag{3.20}$$

Here, Q is a projection operator that requires both particles to be above the Fermi sea, and e is defined by

$$e|\mathbf{k}_1\mathbf{k}_2\rangle = [E(\mathbf{k}_1) + E(\mathbf{k}_2) - E(m) - E(n)]|\mathbf{k}_1\mathbf{k}_2\rangle , \tag{3.21}$$

where $|\mathbf{k}_1\mathbf{k}_2\rangle$ is the product of two single-particle plane waves, and the single-particle energy

$$E(k) = \hbar^2 k^2/2M + U(k) \tag{3.22}$$

depends on the choice of U. The two-hole–line contribution to the energy is given by

$$D_2 = \tfrac{1}{2}A^{-1} \sum_{m,n<k_F} \langle mn|G|mn\rangle , \tag{3.23}$$

and is represented by the diagram in Fig. 14. The two-hole–line approximation to the two-particle excitation amplitude S_2 is

$$\langle ab|S_2^{(2)}|mn\rangle = -\langle ab|(Q/e)G|mn\rangle \tag{3.24}$$

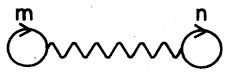

FIG. 14. Diagram representing the two-hole–line contribution D_2 in the Brueckner–Bethe method.

and is represented by the diagram in Fig. 15. Note that Eqs. (3.23) and (3.24) both depend on the choice of U, which is discussed below.

Plausibility arguments for the usefulness of the hole–line expansion are based on the smallness of the parameter κ defined by

$$\kappa = \rho \overline{\int |\phi_{mn} - \psi_{mn}|^2 d\tau} , \tag{3.25}$$

where the bar indicates an average over states m, n in the Fermi sea, and ρ is the density. The integral in Eq. (3.25) can be thought of as a correlation volume, and if $\kappa \ll 1$ then this correlation volume is much smaller than the volume per particle. Every additional hole line in a diagram for either ϵ or ψ_{mn} involves an integration over the Fermi sea giving roughly a factor k_F^3, which is proportional to ρ. On dimensional grounds this factor will be multiplied by a volume, and it is reasonable to expect this volume to be comparable to the integral in Eq. (3.25). Thus an additional hole line is expected to reduce any contribution to $\mathcal{E}$ or ψ_{mn} by roughly a factor κ (Brandow, 1966; Day, 1967).

This argument is quite convincing for short-range correlations caused by the strong short-range repulsion in the nuclear force. For longer-range correlations (equivalently, for virtual excitations to states just above the Fermi surface) it may be necessary to depart from the strict hole–line expansion (Brandow, 1966). How the hole–line expansion can be modified to take account of such correlations is discussed in Sec. III.B.

Since κ is defined in terms of the exact two-body wave function, it is independent of the approximation scheme. Any approximation to ψ_{mn} gives a corresponding approximation to κ. We denote by κ_2 the approximation obtained by using $\psi_{mn}^{(2)}$ in Eq. (3.25). Most previous work follows Brandow (1966) in using the symbol κ for our κ_2. However, it seems preferable to base a general discussion on the quantity κ, which is independent of any approximations used, rather than on κ_2, which depends on the choice of the single-particle potential U. If the hole–line idea leads to a useful approximation, then we will have $\kappa_2 \approx \kappa$, and both quantities will be small compared to 1. For the Reid potential, near the empirical saturation density ($k_F \cong 1.36$ fm^{-1}), and with the conventional choice of U (to be discussed below), one finds $\kappa_2 = 0.15$.

The leading contributions to the energy per particle are the kinetic energy of the Fermi sea, given by the first term in Eq. (3.17), and the two-hole–line contribution D_2 given by Eq. (3.23). Typical numerical values

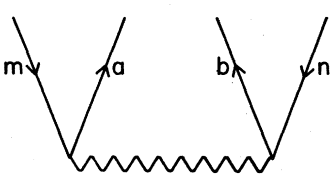

FIG. 15. Diagram representing the lowest-order contribution to $\langle ab|S_2|mn\rangle$.

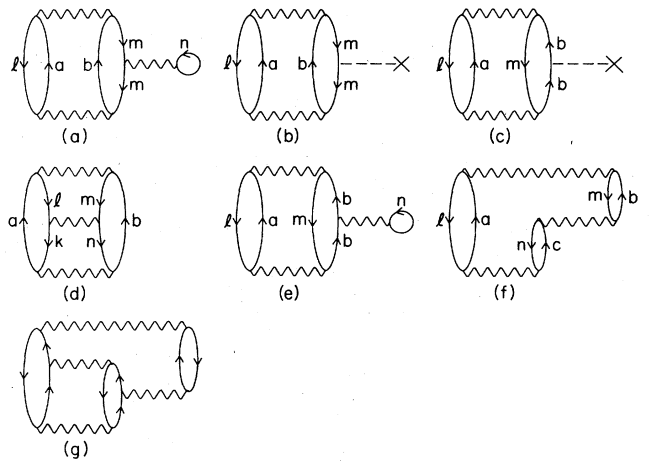

FIG. 16. Low-order three-hole–line diagrams of the Brueckner–Bethe method.

are +25 MeV for the kinetic energy and −35 MeV for D_2. Some three-hole–line diagrams are shown in Fig. 16. Each wiggly line represents a matrix element of G. The dashed line with a cross at the end represents the single-particle potential U. Upgoing lines represent occupied states above the Fermi sea, and downgoing lines represent empty states, or holes, in the Fermi sea. Each intermediate state between interactions contributes an energy denominator given by the sum of the particle energies minus the hole energies. The energy denominators and G matrices both depend on the choice of U. Detailed rules for diagram contributions are given by Day (1967). Diagrams 16a and 16d have four hole lines, but in each case, because of momentum conservation in the middle interaction, only three of the hole momenta are independent. In grouping diagrams according to the number of hole lines, we count each U interaction as one hole line. This keeps terms of the same order of magnitude together. The four-hole–line diagrams have been enumerated by Day (1969) and by Schucan and Weidenmüller (1971).

Figures 16a–16f show all three-hole–line diagrams of third order in powers of G and U. Figures 16e and 16f are the first two members of a class of infinitely many three-hole–line diagrams called three-body cluster diagrams. There are four three-body cluster diagrams of fourth order (one of which is shown in Fig. 16g), eight of fifth order, etc. These diagrams must be summed by solving the Bethe–Faddeev three-body equations (Bethe, 1965; Day, 1967; Rajaraman and Bethe, 1967; Dahlblom, 1969). The three-body cluster diagrams together with diagrams 16a–16d, account for all three-hole–line diagrams.

The contribution D_3^b of the hole–bubble diagram of Fig. 16a is

$$D_3^b = -A^{-1} \sum_{\substack{a,b>k_F \\ l,m,n<k_F}} \langle lm|G(Q/e)|ab\rangle \langle ab|(Q/e)G|lm\rangle \times \langle mn|G|mn\rangle . \quad (3.26)$$

We see from Eq. (3.19) that

$$(Q/e)G|lm\rangle = (Q/e)G\phi_{lm} = \phi_{lm} - \psi_{lm}^{(2)} , \quad (3.27)$$

and this allows $\sum_{a,b}$ in Eq. (3.26) to be done by closure to give

$$D_3^b = -A^{-1} \sum_{l,m,n<k_F} \langle mn|G|mn\rangle \int |\phi_{lm} - \psi_{lm}^{(2)}|^2 d\tau . \quad (3.28)$$

We approximate the integral in (3.28) by its average over l,m. The sum over l then gives a factor ρ, and we find

$$D_3^b \cong -\kappa_2 A^{-1} \sum_{m,n<k_F} \langle mn|G|mn\rangle = -2\kappa_2 D_2 . \quad (3.29)$$

This formula, which is accurate to 20%–30%, shows how the size of κ_2 controls the relative size of D_2 and D_3^b.

Typical values near the saturation density are $\kappa_2 \approx 0.15$ and $D_2 \approx -35$ MeV, so that $D_3^b \approx +10$ MeV. This large term will be canceled by the contribution from diagram 16b if $U(m)$ is chosen properly for $m < k_F$. This motivates the choice

$$U(m) = \sum_{n<k_F} \langle mn|G|mn\rangle , \quad m < k_F \quad (3.30)$$

which causes diagrams 16a and 16b to exactly cancel. All higher-order diagrams with bubble insertions in hole lines are also canceled. The hole–hole contribution D_3^{hh} of Fig. 16d is ≤0.5 MeV in magnitude (Day, 1969) and is relatively unimportant. For $b > k_F$, one could choose $U(b)$ so that the particle–bubble diagram 16e is canceled by diagram 16c. However, diagram 16e is just one diagram of the infinite series that is summed by the Bethe–Faddeev integral equation to give the three-body cluster term D_3^c (Bethe, 1965; Day, 1967; Rajaraman and Bethe, 1967). Diagrams 16f and 16g are other members of this series. Thus it is the complete three-body cluster contribution D_3^c that is important rather than diagram 16e alone. The calculation of Dahlblom (1969) using the Reid potential gave a very small result for D_3^c, only about −1 MeV. This motivated the conventional choice $U(b) = 0$ for $b > k_F$: it is convenient and was expected to give a small three-hole–line contribution. More recent calculations, to be described later, give $D_3^c \approx -4$ MeV, which is acceptably small but not negligible. The choice of $U(b)$ for $b > k_F$ will be discussed more fully later. The single-particle spectrum is plotted in Fig. 17. Since D_3^b is canceled by Fig. 16b, and D_3^{hh} is so small, the only significant contribution to D_3 is the three-body cluster term D_3^c. It is expected to be no larger in magnitude than $\kappa_2 D_2$, and detailed calculations are consistent with this. Thus the relative size of the three-hole–line and two-hole–line terms is roughly determined by κ_2. We see from Eq. (3.25) that κ_2 is an increasing function of density, so that the convergence of the hole–line expansion becomes worse as the density increases.

The four-hole–line diagrams have been enumerated and partially calculated (Day, 1969). Most of them can be reliably estimated at the empirical saturation density to be only a few hundredths of an MeV and hence negligible. There are five terms larger than 0.2 MeV in magnitude, and their sum was estimated to be ~−1 MeV at the empirical density. This contribution is roughly $\kappa_2^2 D_2$ and is consistent with a rate of convergence governed by κ_2. There is one important uncertainty, however. In the four-body-cluster term D_4^c and in another

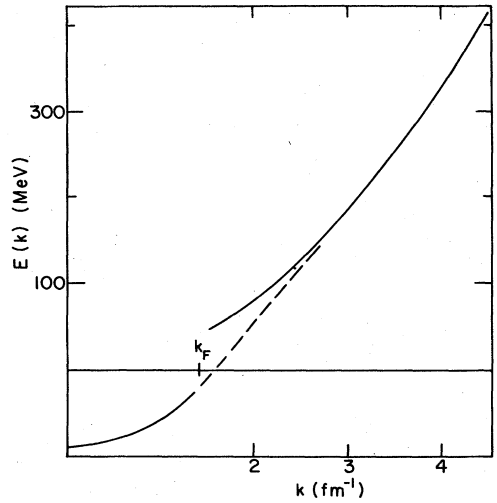

FIG. 17. The single-particle spectrum of the Brueckner–Bethe method. For $k > k_F$ the solid curve is pure kinetic energy. The dashed curve is an example of a spectrum with a smaller gap at the Fermi surface.

term called $B1$ by Day (1969), the tensor force was omitted. Especially in term $B1$, which we denote $D_4(B1)$, the tensor force must be included before the total four-hole–line contribution D_4 can be accurately known. Note also that the estimate of -1 MeV for D_4 is for $k_F = 1.36$ fm^{-1}. At higher densities the magnitude of D_4, and hence the uncertainty in any feasible calculation based on the hole–line expansion, will almost certainly be larger. For a very rough guess, we may assume that both κ and D_2 vary as k_F^2, and that $D_4 \approx \kappa^2 D_2$. Then if $D_4 = -1$ MeV at $k_F + 1.36$ fm^{-1}, we would have $D_4 \approx -5$ MeV at $k_F = 1.8$ fm^{-1}.

We have so far discussed $\mathcal{E}$ and κ, which are defined independently of any approximations and can be calculated if the exact two-body wave function ψ_{mn} is known. Another interesting quantity that is independent of the approximation scheme is the average occupation probability $\bar{n}$ of a single-particle state in the Fermi sea, defined by

$$\bar{n} = \overline{\langle \Psi | a_m^\dagger a_m | \Psi \rangle / \langle \Psi | \Psi \rangle}, \tag{3.31}$$

where Ψ is the exact ground-state wave function, and the bar indicates an average over momenta $m < k_F$. We will see in Sec. III.B that consideration of $\bar{n}$ is useful in testing the validity of the hole–line expansion.

Knowledge of ψ_{mn} does not completely determine $\bar{n}$, but there is a useful diagram expansion for $\bar{n}$ (Brandow, 1967, p. 786). It consists of all linked diagrams in which the operator $a_m^\dagger a_m$ acts exactly once. In the free Fermi-gas state we have $\bar{n} = 1$, and the leading (two-hole–line) correction to this result is given by the diagram of Fig. 18, whose contribution to $\bar{n}$ is $-\kappa_2$. Hence

$$(1 - \bar{n})_2 = \kappa_2, \tag{3.32}$$

where $(1 - \bar{n})_2$ is the two-hole–line contribution to $(1 - \bar{n})$. If the approximation scheme is accurate, we will have $(1 - \bar{n})_2 \cong (1 - \bar{n})$, so that $\kappa_2 \cong 1 - \bar{n}$.

The relation $\kappa_2 \cong 1 - \bar{n}$ allows us to rewrite Eq. (3.29) in the form

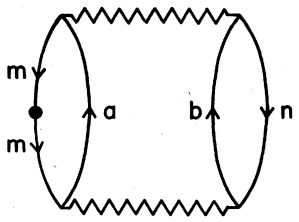

FIG. 18. Two-hole–line contribution to $\bar{n}$. The heavy dot represents the operator $a_m^\dagger a_m$.

$$D_3^b \cong -2D_2(1 - \bar{n}). \tag{3.33}$$

This formula, along with the corresponding diagram 16a, admits the following physical interpretation. The factor $(1 - \bar{n})$ is the probability that a particle is excited from state m in the Fermi sea to state b above the sea, as in the lowest interaction of Fig. 16a. While above the sea, the particle cannot participate in the interaction $\sum_{n<k_F} \langle mn | G | mn \rangle$, represented by the middle interaction in Fig. 16a. The average over states $m < k_F$ of this lost interaction is $A^{-1} \sum_{m,n<k_F} \langle mn | G | mn \rangle$, which is precisely the factor $2D_2$ in Eq. (3.33). So the hole–bubble diagram 16a accounts for the fact that virtual excitations deplete the Fermi sea and thus reduce the energy by an amount proportional to D_2. While the particle is above the Fermi sea, it can of course interact, and these interactions affect the energy through D_3^c, represented by Figs. 16e, 16f, 16g, ... These physical ideas underlie the so-called dispersion effect, which is discussed in Sec. IV.

Let us summarize the results of this subsection. Presently available calculations within the Brueckner–Bethe method are based on the hole–line expansion. If the parameter κ defined by Eq. (3.25) is small compared to 1, then arguments for the accuracy of the hole–line expansion can be made. These arguments are convincing for short-range correlations, but whether they are valid for longer-range correlations remains to be seen. Numerical calculations show that the first two terms of the hole–line expansion behave well. For the Reid potential, near the empirical saturation density, the two-hole–line contribution is -35 MeV, and the three-hole–line contribution is only -4 MeV. Four-hole–line and higher terms have not been accurately calculated.

It is essential to carefully test the validity of the hole–line expansion and of any proposed modification of it. Ways of doing this are discussed in the next subsection.

B. Tests of the Brueckner-Bethe method

In this section we discuss several tests of the validity of the hole–line expansion. A possible modification of the hole–line expansion that takes better account of long-range correlations is also outlined. Finally, for the Reid potential, which has all the complications required to fit the two-body scattering data and deuteron properties, the comparison between available Brueckner–Bethe and variational results is briefly discussed.

Let us first consider the choice of single-particle spectrum. The conventional choice has $U(b) = 0$ for $b > k_F$. This produces a discontinuity, or gap, in the spectrum of about 50 MeV at the Fermi surface (see Fig. 17). For this reason, the conventional choice of spectrum has often been criticized (Jeukenne *et al.*,

1975; Köhler, 1973). Which spectrum is the right one? Since the spectrum is introduced only for calculational convenience, and has no direct physical significance, there is no unique answer to this question.

However, one requirement on the choice of U is that the condition $\kappa_2 \ll 1$ remain valid. This is because, if the hole–line expansion is to be useful, it is necessary to have both $\kappa \ll 1$ and $\kappa_2 \approx \kappa$, which implies $\kappa_2 \ll 1$. An example of a spectrum that does not satisfy this condition is a pure kinetic-energy spectrum, which gives $\kappa_2 \approx 0.5$ for the Reid potential near the empirical saturation density. The conventional spectrum gives $\kappa_2 \approx 0.15$ for this case, and a spectrum with a smaller gap, similar to the dashed line in Fig. 17, gives $\kappa_2 \approx 0.20$ (Köhler, 1973). It is of course conceivable that, for the conventional spectrum, κ_2 is small compared to 1 but κ is not, in which case κ_2 is a bad approximation to κ, and the hole–line expansion will not be useful. If this is the case, it should be discoverable through the tests discussed below.

The exact value of the energy or of any other observable quantity is of course independent of the choice of spectrum. Changing the spectrum redistributes the energy among the various terms in the expansion but leaves the final result the same. We can use this fact to formulate a test of any proposed approximation scheme. Suppose the combination of a particular spectrum and approximation scheme gives an accurate expansion for the energy. Then a new spectrum that differs only slightly from the old one will also provide an accurate energy expansion. In any finite order of approximation, the old and new spectra will give different results, but this difference should rapidly become smaller as the calculation is pushed to higher order. We can test any chosen spectrum and approximation scheme by checking numerically whether or not this requirement is satisfied.

A convenient way to make a small change in the spectrum is to shift $U(b)$ by a constant Δ for $b > k_F$, while keeping $U(m)$ unchanged for $m < k_F$. The derivative with respect to Δ of the calculated energy is then a measure of its sensitivity to Δ. According to the above discussion, this derivative should become rapidly smaller as more terms are included in the expansion for the energy. This idea was first suggested by Mahaux (1971) as a test of the hole–line expansion.

In any order of the hole–line expansion, the derivative with respect to Δ of the calculated energy is related to the quantity $\bar{n}$ defined by Eq. (3.31). If the hole–line expansion for $1-\bar{n}$ is

$$1-\bar{n} = \sum_{h=2}^{\infty} (1-\bar{n})_h , \tag{3.34}$$

then one can show that

$$\frac{\partial}{\partial \Delta}(D_2 + D_3 + \cdots + D_h) = (1-\bar{n})_h . \tag{3.35}$$

Thus insensitivity of the calculated energy to the spectrum is equivalent to convergence of the hole–line expansion for the quantity $(1-\bar{n})$. This is an additional reason to require the calculated energy to be insensitive to small changes in the spectrum. If the hole–line expansion is working, both sides of (3.35) should tend rapidly to zero with increasing h. At the two-hole–line level, since $(1-\bar{n})_2 = \kappa_2$, Eq. (3.35) gives

$$\frac{\partial D_2}{\partial \Delta} = \kappa_2 . \tag{3.36}$$

To carry out this test, we must calculate at least one term beyond the two-hole–line contribution D_2. This requires solving the Bethe–Faddeev equations (Rajaraman and Bethe, 1967; Dahlblom, 1969; Day *et al.*, 1972; Grangé, 1975) to obtain the three-body cluster term D_3^c. If these three-body equations can be solved, one can also calculate all the four-hole–line terms except the four-body cluster D_4^c (Day, 1969). With central forces, D_4^c has been approximately calculated to be -0.1 MeV at the empirical saturation density (Day, 1969; Lassey and Sprung, 1971). Similar methods are available to make an estimate that partially includes the tensor force (Dahlblom, 1969; Lassey and Sprung, 1971; Grangé, 1975). Assuming, as seems probable, that a fairly crude approximation will suffice for D_4^c, an accurate method for solving the three-body equations allows one to calculate all the three- and four-hole–line terms. Thus the ability to solve the three-body equations allows one to go quite far in testing the hole–line expansion. I have found that three-body calculations with the most general nuclear force can be carried out using the method of Day, Coester, and Goodman (1972). The Pauli operator is approximated by angle averaging, and this causes a numerical uncertainty of several tenths of an MeV in D_3^c at $k_F = 1.5$ fm^{-1}. This error is small enough that it is feasible to carry out meaningful tests of the hole–line expansion.

We now summarize the available numerical results on the test of the hole–line expansion described above in connection with Eq. (3.35).

Mahaux (1971) studied the effect of a constant shift in the spectrum and concluded that the sensitivity of the calculated energy was greatly reduced by adding the three-hole–line terms to the lowest-order term. However, since the derivative $\partial D_3^c/\partial\Delta$ of the three-body cluster term had not been calculated at that time, the analysis was incomplete. I have calculated $\partial(D_2+D_3)/\partial\Delta$ by using a method applied previously to S-wave potentials (Day *et al.*, 1972). The calculations have been done for $k_F = 1.5$ fm^{-1}, using the Reid potential, which is defined for two-body partial waves with $j < 3$. The derivative has been evaluated for the conventional spectrum in the following way.

The energy through three-hole–line terms is approximately given by

$$D_2 + D_3 \approx D_2 + D_3^c + D_3^{hh} - 2\kappa_2 D_2 + \kappa_2 \bar{U}_m - \kappa_2 \Delta , \tag{3.37}$$

where we have used the approximation (3.29) for the hole–bubble diagram of Fig. 16a. A similar approximation gives $\kappa_2 \bar{U}_m$ for Fig. 16b, where $\bar{U}_m$ is the average value of $U(m)$ for $m < k_F$. The term $-\kappa_2\Delta$ comes from the potential insertion in a particle line, Fig. 16c. Since we are varying the spectrum above the Fermi sea, $\partial \bar{U}_m/\partial\Delta = 0$. Using this along with $\partial D_2/\partial\Delta = \kappa_2$, one easily finds

$$\frac{\partial(D_2+D_3)}{\partial\Delta} = \frac{\partial D_3^c}{\partial\Delta} - 2\kappa_2^2 + \frac{\partial D_3^{hh}}{\partial\Delta} - (2D_2 - \bar{U}_m + \Delta)\frac{\partial \kappa_2}{\partial\Delta} . \tag{3.38}$$

We want to evaluate this for $\Delta = 0$. For $\Delta = 0$, self-consistency of the hole spectrum gives $2D_2 = \bar{U}_m$, so that the coefficient of $\partial\kappa_2/\partial\Delta$ vanishes, leaving

$$\frac{\partial(D_2+D_3)}{\partial\Delta} = \frac{\partial D_3^c}{\partial\Delta} - 2\kappa_2^2 + \frac{\partial D_3^{hh}}{\partial\Delta} . \tag{3.39}$$

For the Reid potential at $k_F = 1.5$ fm^{-1}, I have found $\partial D_3^c/\partial\Delta = 0.056$. This was obtained by calculating D_3^c for $\Delta = \pm 8.3$ MeV and numerically differentiating. A rough estimate of $\partial D_3^{hh}/\partial\Delta$ gives 0.006. Since $\kappa_2 = 0.168$ at $k_F = 1.5$ fm^{-1}, Eq. (3.39) gives

$$\partial(D_2+D_3)/\partial\Delta = 0.056 - 0.057 + 0.006 = 0.005 . \tag{3.40}$$

This result is only accurate to 0.01 or 0.02, mainly because of the approximate treatment of the contributions from Figs. 16a and 16b. But in any case the result is much smaller than $\kappa_2 = 0.17$, so that including the three-hole–line contribution greatly reduces the sensitivity of the calculated energy to small changes in the single-particle spectrum. Thus the hole–line expansion passes this test.

The numerical results given above were obtained using the conventional spectrum. Calculations using spectra different from the conventional one are also of great interest. Spectra resembling the dashed line of Fig. 17 have been used by Köhler (1973) and by Jeukenne, Lejeune, and Mahaux (1975). If only the two-hole–line term D_2 is included, the calculated energy can be appreciably different from that obtained using the conventional spectrum. For example, for the hard-core potential of Reid (1968) at $k_F = 1.3$ fm^{-1}, Jeukenne *et al.* (1975) find a value of D_2 that is 3.0 MeV more negative with their modified spectrum than with the conventional spectrum.

It would be most helpful if including the three-hole–line terms were to bring the energies calculated with these two quite different spectra much closer together. This is because, if calculations are done to the same order of approximation with both spectra, the uncertainty in the calculation will be at least as large as the difference in the two results, unless convincing arguments can be made that one choice of spectrum gives a more accurate approximation scheme than the other. At present there is no conclusive argument in favor of a particular choice of spectrum. Probably the best approach is that of Zabolitzky (1976b). He proposes that $U(b)$, for $b > k_F$ be chosen so that the lowest-order approximation (3.24) to the pair excitation amplitude S_2 include, as far as possible, the contribution from higher-order terms.

It is thus very important to calculate the three-hole–line and higher terms with modified spectra such as the dashed line of Fig. 17. This requires an accurate calculation of the three-body cluster term D_3^c, which has not yet been made with a modified spectrum. At present the numerical results needed for further investigation of this point are not available.

We have seen in the preceding subsection that knowledge of the pair excitation amplitude $\langle ab|S_2|mn\rangle$, defined as the amplitude in the exact ground state for finding two particles in momentum states a, b above the Fermi sea with two holes in states m, n in the sea, determines the exact ground-state energy. We therefore study the hole–line expansion for S_2. The two-body approximation to S_2 is given by Eq. (3.24) and is represented by the diagram of Fig. 15.

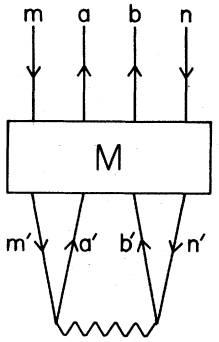

FIG. 19. Diagram representing the three-body cluster contribution to $\langle ab|S_2|mn\rangle$.

The three-hole–line contribution to S_2 is obtained by removing the topmost interaction from each three-hole–line energy diagram. With the conventional spectrum, D_3^c gives the dominant three-hole–line contribution. The corresponding contribution to S_2 is represented by the diagram in Fig. 19. The block represents an operator, or matrix, M that takes the two-hole–line contribution to S_2 into the three-hole–line contribution to S_2. The diagram expansion for M is shown in Fig. 20. Summing this series for M requires solving the Bethe–Faddeev three-body equation (Rajaraman and Bethe, 1967; Dahlblom, 1969; Day *et al.*, 1972; Grangé, 1975) and integrating the result over the coordinates of the third particle.

Once M has been obtained, it may be applied once, twice, etc., to $S_2^{(2)}$ to generate the three-hole–line contribution to S_2 and a selected sequence of 4, 5, . . . -hole–line contributions. Each diagram for S_2 gives a contribution to the energy if a G matrix is added at the top to de-excite the particles. Applying M once, followed by a G matrix, gives the three-body cluster term D_3^c. Applying M twice, followed by a G matrix, gives the four-hole–line contribution $D_4(B1)$. This contribution was calculated by Day (1969) for central forces but has never been calculated for nuclear matter with tensor forces included. It is this four-hole–line term that most ur-

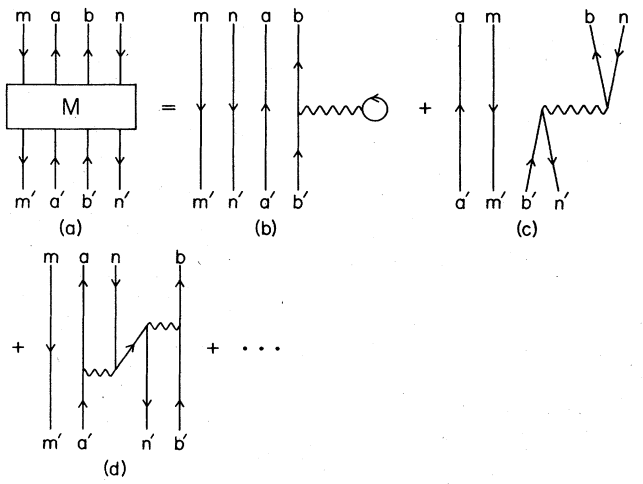

FIG. 20. Diagrammatic representation of the matrix M, as described in the text.

gently needs investigation. Using the relation

$$M+M^2+M^3+\cdots=M(1-M)^{-1}, \tag{3.41}$$

we see that the entire series of contributions, to either S_2 or the energy, can be summed by inverting the matrix $(1-M)$. Modifying the hole–line expansion by doing this partial summation has been suggested before (Lührmann, 1977; Kümmel *et al.*, 1978) and has been carried out for light nuclei (Zabolitzky, 1974). This partial sum is the most likely place to look for possible effects of long-range correlations caused by the tensor force. Repeated application of the matrix M can build these up if they actually exist. Note that the particle–bubble and ring vertices are both included in M (Figs. 20b and 20c), so the partial summation includes all iterations of these. Such terms give important long-range correlations for Bose systems and for the electron gas. It seems sensible, therefore, to investigate their effect in nuclear matter too. We call the resulting sequence of diagrams the generalized ring diagrams. [The diagrams just described include all "forward-going" ring diagrams. For Bose systems and the electron gas, "backward-going" ring diagrams also give important long-range correlations. These are included in the last term of Eq. (3.43) below].

The most favorable result would be that each term in Eq. (3.41) is smaller than the preceding term by a factor κ_2. This would be consistent with the hole–line expansion because each term in Eq. (3.41) involves one more hole line than its predecessor. In particular, the four-hole–line term $D_4(B1)$ would be smaller than the three-body cluster term D_3^c by a factor κ_2. On the other hand, if the successive terms in Eq. (3.41) do not fall off rapidly, this would mean the hole–line expansion is inadequate for these long-range correlations. It would then be necessary to modify the hole–line expansion by evaluating $(1-M)^{-1}$ to obtain the entire sum at once, as suggested earlier by Lührmann (1977) and Kümmel *et al.* (1978).

In the latter case, additional modification of the hole–line expansion is required. The situation can be understood with the aid of the exact equation [derived from the results of Coester (1969]

$$S_2=-Q/eG+MS_2+S_2', \tag{3.42}$$

whose solution is

$$S_2=-Q/eG-M(1-M)^{-1}Q/eG+(1-M)^{-1}S_2'. \tag{3.43}$$

Here, S_2' is a functional of S_2 and of the linked amplitudes S_3 and S_4. Evaluating the second term in Eq. (3.43), without truncating the series $(1-M)^{-1}=1+M+\cdots$, sums the generalized ring diagrams and departs from the strict classification of terms according to the number of hole–lines. If this is necessary for the second term in Eq. (3.43), it will presumably be necessary for the third term as well. The second term in Eq. (3.43) is expected to be much more important than the third term. The leading contribution to the energy from the second term is the three-body cluster term D_3^c. The leading energy contributions from the third term, with the exception of the unimportant hole–hole term D_3^{hh}, all involve four hole lines. The work of Day (1969) gives evidence that the sum of these terms is much smaller than the contribution of about −4 MeV from D_3^c.

We now summarize the available numerical evidence on the convergence of the generalized ring series of Eq. (3.41). The sum of ring diagrams has been studied by Dahlblom and Kouki (1971) and by Clement (1973). Two simplifications were made: The full matrix M was replaced by the ring vertex of Fig. 20c alone, and the reaction matrix in this vertex was replaced by the truncated one-pion exchange potential given by

$$v(\mathbf{r})=v_{\mathrm{OPEP}}\ ,r>d$$

$$=0\ ,r<d. \tag{3.44}$$

Recall that v_{OPEP} contains a strong tensor component. The cutoff radius d was varied from 0.8 to 1.4 fm^{-1}. The sum of all ring diagrams with four or more hole lines was found to be roughly half the three-hole–line ring contribution. But a calculation using the correct matrix M remains to be done for nuclear matter. For the light nucleus ^{16}O the full calculation *has* been done by Zabolitzky (1974). The contribution to the energy from generalized ring diagrams with four or more hole lines, for ^{16}O with the Reid potential, was about 40% of the three-body cluster contribution. If the same ratio persists in nuclear matter, the generalized rings with four or more hole lines would contribute about −1.5 MeV at the empirical saturation density. The generalized ring contribution may well be larger than this, for two reasons. First, the density of nuclear matter is larger than the average density of ^{16}O. Second, there is more room for the buildup of long-range ring correlations in nuclear matter than in the rather small nucleus ^{16}O.

Thus published numerical results give some indication that summing the generalized ring diagrams may be essential. But a proper calculation for nuclear matter remains to be done. The tests of the hole–line expansion considered above all are internal checks: The hole–line calculations themselves are used in making the tests. A completely different, and very valuable, test would be to compare Brueckner–Bethe results against results obtained by some other method that is known to be accurate. For simple central potentials, we have seen that the Fermi hypernetted-chain (FHNC) calculations give accurate upper bounds to the energy. So an excellent test is to compare Brueckner–Bethe and FHNC results for such potentials.

This comparison was made for several central potentials in Sec. II.C (see Figs. 9–11). Only the two-body Brueckner–Bethe results, calculated with the conventional spectrum, are available. The Brueckner–Bethe results lie above the FHNC upper bounds in all cases, but the exact results must lie slightly below the FHNC results. So the question arises of whether the higher-order terms in the hole–line expansion can make up these differences. The three-body contribution is expected to be of the order of $\kappa_2 D_2$, and error bars of this size are shown for the Brueckner–Bethe results in Figs. 9–11. We see that corrections of this order of magnitude would be sufficient to make the hole–line results consistent with the FHNC results. It is essential that the three- and four-hole–line terms be evaluated to see whether agreement is obtained. At present we can only say that the comparison gives no cause for alarm.

So far I have calculated the three-hole-line contribution only for the Reid potential, which is defined in two-body partial waves with $j<3$. The three-body cluster term was calculated using a method applied earlier to S-wave potentials (Day *et al.*, 1972). The conventional spectrum was used, and the results are shown in Fig. 13. The curve labeled $BB(2)$ gives the two-body result. Adding the three-hole–line contribution $D_3^c + D_3^{hh}$ gives the curve labeled $BB(2+3)$. Since the four-hole–line calculations are incomplete, we can only guess their contribution. The dashed line labeled $BB(2+3+4)$ is obtained by adding one such guess to the three-hole–line result. In this guess, we assume that D_4^c and $D_4(B1)$ give -0.2 and -0.7 MeV, respectively, at $k_F = 1.4$ fm^{-1}, and that both contributions are proportional to k_F^6. All other four-hole–line terms are estimated using the formulas of Day (1969). The resulting dashed curve saturates at $k_F = 1.54$ fm^{-1}. However, we have seen that $D_4(B1)$ and the other generalized ring diagrams could be several times larger than the above guess. In that case, the calculated saturation point might be shifted to the region $k_F > 1.6$ fm^{-1}.

Reid (1968) does not give a potential in two-body partial waves with $j \geq 3$. The Brueckner–Bethe results must be extended to include the effect of a potential that is consistent with empirical phase shifts in these partial waves. These partial waves have been found to contribute +0.7 MeV to the two-hole–line term D_2 at the empirical saturation density (Sprung *et al.*, 1970). This result does not permit an estimate of their contribution to D_3^c. However, in partial waves with sufficiently large j, only the long-range component of the two-body potential, i.e., the one-pion exchange potential (OPEP), is relevant. Since the spin-isospin average of OPEP is zero, it is unlikely that partial waves with $j \geq 3$ will contribute much to D_3.

The comparison of the Brueckner–Bethe and variational results shown in Fig. 13 is encouraging in one respect. At any give value of k_F below 1.6 fm^{-1}, the Brueckner–Bethe energy is reasonably close to the lower of the two variational curves. However, the variational calculation saturates at a much higher density than the Brueckner–Bethe calculation. As discussed above, a proper calculation of the generalized ring diagrams may also shift the saturation point of the Brueckner–Bethe result to higher density.

We remark here that the three-hole–line contribution moves the hole– line result for the Reid potential closer to the empirical saturation point. This is seen in Fig. 21, where saturation points obtained from two-hole–line calculations using the conventional spectrum are shown for a number of two-body potentials that fit nucleon–nucleon scattering data. The two-hole–line saturation points lie on a narrow band (called the Coester band) that does not include the empirical saturation point, which lies inside the open rectangle. The three-hole–line contribution moves the Reid saturation point off the band and closer to the empirical region. However, as we have seen, it is not yet known whether higher-order contributions will appreciably shift this saturation point.

In summary, we have suggested three tests for the validity of the hole–line expansion. First, the sensitivity of the calculated energy to small changes in the spectrum must rapidly decrease as successive terms are included in the expansion. Second, the sum of generalized ring diagrams should converge well. Third, the hole–line expansion should be consistent with variational results for simple central potentials, which are known to be accurate. These tests are, of course, not completely independent of each other. If the generalized rings do not converge well, i.e., if the generalized rings with four or more hole lines give a contribution comparable to the three-body cluster term, then the hole–line expansion would be inaccurate. In that case, the generalized rings could be summed in closed form, as suggested earlier (Lührmann, 1977; Kümmel *et al.*, 1978). With this modification, the sensitivity of the calculated energy to the spectrum, and the agreement of Brueckner–Bethe results with variational results for simple potentials, could again be tested to see whether this modified method is satisfactory.

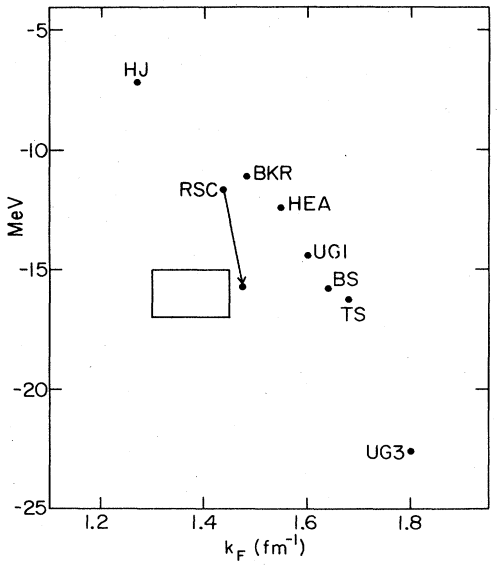

FIG. 21. Saturation points calculated with the Brueckner–Bethe method, including the two-hole–line term with the conventional spectrum. Further information is given in Table II. The arrow shows the shift in the saturation point for the Reid potential when three-hole–line terms are included. The empirical saturation point lies in the open rectangle.

All these tests can be carried out using numerical techniques that are presently available. Assuming that a well-founded approximation scheme emerges, how accurately can we calculate the energy with the Brueckner–Bethe method? With our present computational ability, we cannot expect an uncertainty smaller than $\kappa_2^2 D_2$, where D_2 is the two-body contribution. For the Reid potential, this gives errors of order 1 MeV at $k_F = 1.4$ fm^{-1} and 5 MeV at $k_F = 1.8$ fm^{-1}. Thus the present version of the Brueckner–Bethe method, which relies on κ being small, begins to break down at high densities. If it is really true, as the variational calculations suggest, that the Reid potential gives saturation only at some very high density near $k_F = 2.0$ fm^{-1}, then a different version of the Brueckner–Bethe method would be required in order to locate this saturation point.

TABLE II. Authors of the nucleon–nucleon potentials and nuclear matter calculations shown in Fig. 21.

Symbol	Authors of potential	Nuclear matter calculation by
HJ	Hamada and Johnston[a]	Banerjee and Sprung[b]
BKR	Bressel, Kerman, and Rouben[c]	Banerjee and Sprung[b]
RSC	Reid[d]	Coester, Pieper, and Serduke[e]
HEA	Holinde, Erkelenz, and Alzetta[f]	Holinde, Erkelenz, and Alzetta[f]
UG1	Ueda and Green[g] Model 1	Wong and Sawada[h]
UG3	Ueda and Green[g] Model 3	Coester, Pieper, and Serduke[e]
BS	Bryan and Scott[i]	Wong and Sawada[h]
TS	DeTourreil and Sprung[j]	DeTourreil and Sprung[j]

[a]Hamada, T., and I. D. Johnston, 1962, Nucl. Phys. **34**, 382.
[b]Banerjee, P. K., and D. W. L. Sprung, 1971, Can. J. Phys. **49**, 1871.
[c]Bressel, C., A. Kerman, and B. Rouben, 1969, Nucl. Phys. A **124**, 624.
[d]Reid (1968).
[e]Coester, F., S. C. Pieper, and F. J. D. Serduke, 1975, Phys. Rev. C **11**, 1.
[f]Holinde, K., K. Erkelenz, and R. Alzetta, 1972, Nucl. Phys. A **198**, 598.
[g]Ueda, T., and A. E. S. Green, 1968, Phys. Rev. **174**, 1304.
[h]Wong, C. W., and T. Sawada, 1972, Ann. Phys. (N.Y.) **72**, 107.
[i]Bryan, R., and B. L. Scott, 1969, Phys. Rev. **177**, 1435.
[j]DeTourreil, R., and D. W. L. Sprung, 1973, Nucl. Phys. A **201**, 193.

IV. DISCUSSION

In this section we summarize and discuss the present situation and consider prospects for the future. The most firmly established results are those of the variational method for central potentials. Variational calculations are much easier for central potentials than for the very complicated nuclear potential. For central forces, there is little doubt that the FHNC and Monte Carlo methods give accurate energy expectation values with reliable error estimates that are usually 2 MeV or smaller. The two-body Brueckner–Bethe calculations with the conventional spectrum lie consistently above these variational upper bounds. This is usually attributed to the dispersion effect. Let us now discuss this idea, which I believe is indeed correct.

We first recall the interpretation given in Sec. III.A of the Brueckner–Bethe hole–bubble diagram (Fig. 16a), whose contribution to the energy is approximately $-2\kappa_2 D_2$. This represents the loss in binding when a particle in the Fermi sea is excited to a state above the sea. The factor κ_2 gives the probability of excitation, and the interaction energy of one particle in the sea with all the others is $2D_2$. The conventional choice of spectrum takes this effect into account by canceling the hole-bubble diagram against diagram 16b, which has a single-particle potential insertion in a hole line.

What does the particle do when it is above the Fermi sea? The conventional spectrum puts $U(b)=0$ for $b>k_F$, thus assuming that the interaction energy of a particle above the sea is zero. However, if a particle above the sea interacts with the others just as effectively as when it is in the sea, then we would have an additional contribution $2\kappa_2 D_2$ to the energy. This quantity is called the dispersion term. How the particle actually interacts with the others while above the sea is determined by the Brueckner–Bethe three-body cluster term (possibly modified by inclusion of the generalized ring contributions discussed in Sec. III.B). In most cases this three-body term will be between the extremes of zero and $2\kappa_2 D_2$. For example, for the Reid potential at $k_F=1.4$ fm^{-1}, $D_3^c\approx -4$ MeV and $2\kappa_2 D_2\approx -10$ MeV.

Thus, within the context of the Brueckner–Bethe hole-line expansion, a two-body calculation is expected to give too little binding by an amount somewhere between zero and the dispersion term $2\kappa_2 D_2$. To pin this number down more accurately requires calculating the three-body cluster term. Error bars of size $\kappa_2 D_2$ are shown on the graphs of most two-body Brueckner–Bethe results in this paper. One sees in Figs. 9–11 that inclusion of the three-body term may well repair the discrepancies between two-body Brueckner–Bethe results and the reliable variational upper bounds for central forces. This will provide a valuable test of the hole-line expansion.

The idea that a two-body Brueckner–Bethe calculation could be in error by roughly $\kappa_2 D_2$ because of the dispersion effect is not a new one. It has simply been lost sight of through a historical accident. Dahlblom's (1969) approximate calculation of the three-body cluster term for the Reid potential gave a small result of only about −1 MeV. Many two-body Brueckner–Bethe calculations were subsequently done on the assumption that the three-body term is negligible. As shown in Fig. 21, the resulting saturation points for a wide variety of potentials lie on a narrow band (the Coester band) in the energy-density plane that does not include the empirical saturation point (Day, 1976). However, we have seen that more accurate calculations with the Reid potential give a three-body contribution of about −4 MeV. Furthermore, including this contribution moves the calculated

saturation point for the Reid potential off the Coester band (see Fig. 21). Thus, at least for the Reid potential, neglecting the three-body term in the hole–line expansion is not permissible. Similarly, for central potentials, if the results of the hole–line expansion are to be brought into agreement with the variational results, the Brueckner–Bethe three-body term will again be appreciable.

Formal comparison of the Brueckner–Bethe hole–line expansion and the variational cluster expansion gives an additional reason to expect the Brueckner–Bethe three-body term to repair the discrepancy. The formal comparison is most easily made when the correlation operator f is chosen so that $f\phi = \psi^{(2)}$, where ϕ is a plane wave and $\psi^{(2)}$ is the Bethe–Goldstone wave function defined by Eq. (3.19). This of course requires f to be a more complicated operator than just a function of r. For this choice of f, Wong (1971) has shown analytically that the two-body cluster energy of the variational method lies below the two-body Brueckner–Bethe result with the conventional spectrum by the dispersion term $2\kappa_2 D_2$. This result is valid for two-body potentials of arbitrary complexity.

Schäfer (1972) and Wong (1977) have extended this result to three-body terms. Suppose that a three-body correlation function is introduced into the variational wave function in such a way that the three-body wave functions in the Brueckner–Bethe and variational calculations are the same. Then Schäfer has shown analytically that the energies of the two methods, calculated through three-body cluster terms, differ only by terms that, in the hole–line classification, have four hole lines. Hence it is plausible that including the Brueckner–Bethe three-body term will greatly reduce the discrepancy that now exists between the two-body Brueckner–Bethe results and the variational results.

Having discussed the dispersion effect in the Brueckner–Bethe method, we now summarize the available methods of testing the reliability of this method. We must first sum the series of generalized ring diagrams, as described in Sec. III.B. This tests whether the hole–line expansion takes proper account of long-range correlations. If the generalized ring series converges well, this indicates that the hole–line expansion is adequate. Otherwise, one has to sum this series (this is feasible with presently available numerical techniques), as has been suggested earlier (Lührmann, 1977; Kümmel *et al.*, 1978).

In either case, two further tests can be applied. First, the Brueckner–Bethe results must agree with the variational results for central potentials, for which the variational results are known to be reliable. Second, the Brueckner–Bethe results must be insensitive to small changes in the single-particle spectrum. If the Brueckner–Bethe method passes both these tests, it will be convincing evidence (but by no means a proof) that the method is reliable.

No calculation is meaningful without an error estimate, and a reasonable error estimate is the size of the last term calculated. It is feasible to accurately calculate all the four-hole–line diagrams except the four-body cluster, for which fairly rough approximations must be made. Assuming the numerical inaccuracy of the four-body cluster is small, the error would then be of the order of 1 MeV at $k_F = 1.4$ fm^{-1} and would rise to several MeV at $k_F = 1.8$ fm^{-1}. To do much better than this would require a better understanding of the Brueckner–Bethe method than we now have.

Let us now turn from the Brueckner–Bethe method to the variational methods. For central potentials, the variational method gives reliable upper bounds that are probably within 2 MeV of the exact ground-state energy. For tensor forces, the accuracy of the energy expectation value is not yet established. Two approaches have been used for tensor forces: evaluation of the cluster expansion through three-body terms (Ristig *et al.*, 1972; Kürten and Ristig, 1977) and summation of selected classes of terms (Pandharipande and Wiringa, 1976; Wiringa and Pandharipande, 1978; Rosati, 1977; Smith, 1977) in analogy to the FHNC procedure, which is so successful for central forces.

In the cluster calculations done so far (Kürten and Ristig, 1977) the parameter κ_J ranges roughly from 0.15 to 0.35 as k_F goes from 1.4 to 1.7 fm^{-1}, and the three-body contribution is always less than 4 MeV, which is surprisingly small. An estimate of the four-body cluster term would be a valuable error estimate for these calculations. It would also be very interesting to have cluster expansion calculations for the Reid potential in order to compare them with Brueckner–Bethe results and with the variational results of Pandharipande and Wiringa. Pandharipande and Wiringa have identified and summed certain important classes of terms, and they along with others (Rosati, 1977; Smith, 1977; Owen, 1977) are continuing this program. How high one can go in density before their approximation breaks down is not yet clear.

Using different treatments of the kinetic energy, which was found in Sec. II.C to give reliable error estimates for central forces, would also be useful in obtaining error estimates for the variational calculations with tensor forces. Thus reliable error estimates for calculated energy expectation values with tensor forces are not yet available. But the method is being rapidly developed, and this situation may improve in the future.

The present disagreement between the Brueckner–Bethe and variational results can be summarized quite simply. For central forces, two-body Brueckner–Bethe results lie consistently above the variational results, which are known to be reliable upper bounds. Since the discrepancy is comparable to the expected size of the three-body Brueckner–Bethe term, it is not alarming. The discrepancy will, of course, *become* alarming if higher-order Brueckner–Bethe calculations do not quantitatively account for it. For the Reid potential, the Brueckner–Bethe result (including two-, three-, and four-hole–line terms) is compared with two recent variational calculations by Pandharipande and Wiringa in Fig. 13. The latter calculations saturate at much higher density ($k_F = 1.9$ fm^{-1}) than the Brueckner–Bethe result of $k_F \lesssim 1.6$ fm^{-1} (the empirical value is $k_F = 1.29$–1.44 fm^{-1}). In both methods, improvements in the calculations may change the numerical results. Inclusion of the generalized ring diagrams may cause the Brueckner–Bethe result to saturate at higher density. And inclusion of additional terms may significantly

change the variational results, with an unknown effect on the saturation density.

We close with some general remarks about the Brueckner–Bethe and variational methods. In the Brueckner–Bethe method, simultaneous correlations among n particles can only be taken into account by solving the n-body Faddeev equations. At present we can calculate reliably only for $n=2$ and 3. This allows us to take account of the long-range correlations represented by the generalized ring diagrams. But correlations in which four particles are simultaneously close enough to each other for all repulsive cores to be touching are taken into account by the four-body cluster term, which requires solving a four-body equation. If such correlations are essential for saturation, a Brueckner–Bethe calculation that solves only two- and three-body equations can be valid only at densities below the saturation density. An example of this kind is liquid ^{3}He, for which the value of κ_2 at saturation is about 0.5, which is too large for a low-order Brueckner–Bethe calculation to be successful. The two-body potential between ^{3}He atoms has a Wigner exchange mixture, i.e., it is the same in all partial waves. For a pure S-wave potential, on the other hand, we know that saturation occurs even for a purely attractive force with no repulsion at all. For a system of bosons interacting through the potential v_2 of Eq. (2.47), treated as a pure S-wave potential, I have calculated the two- and three-hole–line terms and find that saturation occurs at sufficiently low density that κ_2 is small, and the Brueckner–Bethe method can be expected to work. It is expected to work even better for fermions with the same S-wave interaction. The exchange mixture of the nuclear force is somewhere between the two extremes of a Wigner force and a pure S-wave force. Roughly speaking, it is the same in all even partial waves and is very weak in odd partial waves. There is also a tensor force, whose effect on saturation is not very well understood. Thus the saturation mechanism involves not only the short-range repulsion in the two-body potential, but also its weakness in odd states and the tensor force. Hence saturation may occur in nuclear matter at a small enough value of κ that the Brueckner–Bethe method is valid. Only accurate calculations can decide this question.

The variational method has the advantage that n-body correlations can be taken into account without solving an n-body equation. Instead, one has only to integrate over the coordinates of n particles. When the correlation operator is simply a product of functions $f(r)$, the Fermi hypernetted-chain (FHNC) equations allow the most important many-body correlations to be treated in a fairly simple way. The FHNC method is therefore useful at higher densities than the Brueckner–Bethe method. For example, FHNC can be used for liquid ^{3}He (Zabolitzky, 1977). However, for nuclear matter the correlation operator f must contain operators such as the tensor and spin–orbit operators, and this makes the variational calculations immensely more complicated. This is in contrast to the Brueckner–Bethe method, where going from a simple central potential to the most general nuclear force causes only a moderate increase in the complexity of the calculations. Many people (Wiringa and Pandharipande, 1978; Schmidt, 1977; Rosati, 1977; Owen, 1977) are now developing FHNC-type summation methods for correlation functions with operators. The situation is changing rapidly, and it is not yet clear how far one can go with this approach.

Thus the variational method has the possibility of working at higher density than the Brueckner–Bethe method, but taking account of the complicated nature of the nuclear force is simpler in the Brueckner–Bethe method. Finally, we should not forget the Monte Carlo method of evaluating the variational expectation value. The recent extension of this technique to the case of fermions with central forces (Ceperley *et al.*, 1977) is a most useful and interesting development. The Monte Carlo method is applicable to both high and low densities and gives completely reliable error estimates. If it could be extended to the most general nuclear force, it would be superior to both the Brueckner–Bethe method and the FHNC version of the variational method.

In conclusion we remark that, with our present understanding of many-body theory, and with presently available calculational methods, several significant tests can be made of both the Brueckner–Bethe method and of the variational method with tensor forces. When these calculations have been done, we will be in a much better position to judge the validity of both methods.

ACKNOWLEDGMENTS

I am especially grateful to F. Coester and J. Zabolitzky for critically reading the manuscript of the paper. I thank V. R. Pandharipande, R. B. Wiringa, and M. L. Ristig for communicating results before publication. I would also like to thank F. Coester, J. Zabolitzky, B. Brandow, J. Clark, M. Kalos, E. Krotscheck, J. Negele, and M. Peshkin for helpful discussions.

REFERENCES

Bäckman, S. O., D. A. Chakkalakal, and J. W. Clark, 1969, Nucl. Phys. A **130**, 635.
Bäckman, S. O., J. W. Clark, W. J. Ter Louw, D. A. Chakkalakal, and M. L. Ristig, 1972, Phys. Lett. B **41**, 247.
Benhar, O., C. Ciofi degli Atti, S. Fantoni, S. Rosati, A. Kallio, L. Lantto, and P. Toropainen, 1976, Phys. Lett. B 64, 395.
Bethe, H. A., 1965, Phys. Rev. **138**, 804B.
Bethe, H. A., 1971, Annu. Rev. Nucl. Sci. **21**, 93.
Brandow, B. H., 1966, Phys. Rev. **152**, 863.
Brandow, B. H., 1967, Rev. Mod. Phys. **39**, 771.
Brandow, B. H., 1976, Phys. Lett. B **61**, 117.
Brueckner, K. A., 1976, Phys. Rev. C **14**, 1999.
Brueckner, K. A., and J. L. Gammel, 1958, Phys. Rev. **109**, 1023.
Calogero, F., and F. Palumbo, 1973, Nuovo Cimento Lett. **6**, 663.
Campani, E., S. Fantoni, and S. Rosati, 1976, Nuovo Cimento Lett. **15**, 217.
Campi, X., and D. W. Sprung, 1972, Nucl. Phys. A **194**, 401.
Ceperley, D. M., G. V. Chester, and M. H. Kalos, 1976, Phys. Rev. D **13**, 3208.
Ceperley, D. M., G. V. Chester, and M. H. Kalos, 1977, Phys. Rev. B **16**, 3081.
Chakkalakal, D. A., C.-H. Yang, and J. W. Clark, 1976, Nucl. Phys. A **271**, 185.

Clark, J. W., and P. Westhaus, 1966, Phys. Rev. **141**, 833; **149**, 990(E).
Clark, J. W., and P. Westhaus, 1968, J. Math. Phys. **9**, 131.
Clark, J. W., and M. L. Ristig, 1972, Phys. Rev. C **5**, 1553.
Clark, J. W., and M. L. Ristig, 1973, in *The Nuclear Many-Body Problem: Proceedings of the International Symposium on Present Status and Novel Developments in the Nuclear Many-Body Problem, Rome, 1972*, edited by F. Calogero and C. degli Atti (Compositori, Bologna), p. 273.
Clark, J. W., P. M. Lam, and W. J. Ter Louw, 1975, Nucl. Phys. A **255**, 1.
Clement, D. M., 1973, Nucl. Phys. A **205**, 398.
Coester, F., 1958, Nucl. Phys. **7**, 421.
Coester, F., 1969, in *Lectures in Theoretical Physics: Quantum Fluids and Nuclear Matter*, edited by K. T. Mahanthappa and W. E. Brittin (Gordon and Breach, New York), Vol. XI B.
Dahlblom, T. K., 1969, in Proceedings of the Abo Academy (NORDITA, Copenhagen), Ser. B, Vol. 29, No. 6.
Dahlblom, T. K., and T. Kouki, 1971, Nucl. Phys. A **175**, 45.
Day, B. D., 1967, Rev. Mod. Phys. **39**, 719.
Day, B. D., 1969, Phys. Rev. **187**, 1269.
Day, B. D., F. Coester, and A. Goodman, 1972, Phys. Rev. C **6**, 1992.
Day, B. D., and F. Coester, 1976, Phys. Rev. C **13**, 1720.
Fâi, G., and J. Németh, 1973, Nucl. Phys. A **208**, 463.
Fantoni, S., and S. Rosati, 1974, Nuovo Cimento A **20**, 179.
Fantoni, S., and S. Rosati, 1975, Nuovo Cimento A **25**, 593.
Fantoni, S., and S. Rosati, 1976, Nuovo Cimento Lett. **16**, 531.
Gammel, J. L., R. S. Christian, and R. M. Thaler, 1957, Phys. Rev. **105**, 311.
Gammel, J. L., and R. M. Thaler, 1960, in *Progress in Elementary Particle and Cosmic Ray Physics*, edited by J. G. Wilson and S. A. Wouthuysen (North Holland, Amsterdam), Vol. V.
Gaudin, M., J. Gillespie, and G. Ripka, 1971, Nucl. Phys. A **176**, 237.
Goldstone, J., 1957, Proc. R. Soc. Lond. A **239**, 267.
Grangé, P., 1975, Phys. Lett. B **56**, 439.
Iwamoto, F., and M. Yamada, 1957, Prog. Theor. Phys. **18**, 543.
Jackson, H. W., and E. Feenberg, 1961, Ann. Phys. (N.Y.) **15**, 266.
Jeukenne, J.-P., A. Lejeune, and C. Mahaux, 1975, Nucl. Phys. A **245**, 411.
Jeukenne, J.-P., A. Lejeune, and C. Mahaux, 1976, Phys. Rep. C **25**, 84.
Kallio, A., and R. A. Smith, 1977, Phys. Lett. B **68**, 315.
Kalos, M. H., 1970, Phys. Rev. A **2**, 250.
Kalos, M. H., D. Levesque, and L. Verlet, 1974, Phys. Rev. A **9**, 2178.
Kalos, M. H., 1977, Invited Talk at the Workshop on Nuclear and Dense Matter, May 3–6, University of Illinois, Urbana, Illinois.
Köhler, H. S., 1973, Nucl. Phys. A **204**, 65.
Köhler, H. S., 1975, Phys. Rep. C **18**, 217.
Krotscheck, E., 1975, Phys. Lett. A **54**, 123.
Krotscheck, E., 1976, Nuovo Cimento Lett. **16**, 269.
Krotscheck, E., 1977, J. Low Temp. Phys. **27**, 199.
Krotscheck, E., and M. L. Ristig, 1975, Nucl. Phys. A **242**, 389.
Krotscheck, E., and K. Takahashi, 1976a, Phys. Lett. B **61**, 393.
Krotscheck, E., and K. Takahashi, 1976b, Phys. Lett. B **63**, 269.
Kümmel, H., 1976, Z. Phys. **279**, 271.
Kümmel, H., K. H. Lührmann, and J. G. Zabolitzky, 1978, Phys. Rep. C **36**, 1.
Kürten, K. E., and M. L. Ristig, 1977, Phys. Lett. B **66**, 113.
Lassey, K. R., and D. W. L. Sprung, 1971, Nucl. Phys. A **177**, 125.
Lührmann, K. H., 1977, Ann. Phys. (N.Y.) **103**, 253.
Mahaux, C., 1971, Nucl. Phys. A **163**, 299.
Myers, W. D., and W. J. Swiatecki, 1969, Ann. Phys. (N.Y.) **55**, 395.
Negele, J. W., 1970, Phys. Rev. C **1**, 1260.
Ohmura, T., M. Morita, and M. Yamada, 1956, Prog. Theor. Phys. **15**, 222.
Owen, J. C., 1977, private communication.
Owen, J. C., R. F. Bishop, and J. M. Irvine, 1976, Nucl. Phys. A **274**, 108.
Owen, J. C., R. F. Bishop, and J. M. Irvine, 1977, Nucl. Phys. A **277**, 45.
Pandharipande, V. R., 1971, Nucl. Phys. A **178**, 123.
Pandharipande, V. R., and H. A. Bethe, 1973, Phys. Rev. C **7**, 1312.
Pandharipande, V. R., R. B. Wiringa, and B. D. Day, 1975, Phys. Lett. B **57**, 205.
Pandharipande, V. R., and R. B. Wiringa, 1976, Nucl. Phys. A **226**, 269.
Pandharipande, V. R., and K. E. Schmidt, 1977, Phys. Rev. A **15**, 2486.
Rajaraman, R., and H. A. Bethe, 1967, Rev. Mod. Phys. **39**, 745.
Reid, R. V., 1968, Ann. Phys. (N.Y.) **50**, 411.
Ristig, M. L., W. J. Ter Louw, and J. W. Clark, 1971, Phys. Rev. C **3**, 1504.
Ristig, M. L., W. J. Ter Louw, and J. W. Clark, 1972, Phys. Rev. C **5**, 695.
Rosati, S., 1977, Invited Talk at the Workshop on Nuclear and Dense Matter, May 3–6, University of Illinois, Urbana, Illinois.
Schäfer, L., 1972, Nucl. Phys. A **194**, 497.
Schmidt, K. E., 1977, Invited Talk at the Workshop on Nuclear and Dense Matter, May 3–6, University of Illinois, Urbana, Illinois.
Schucan, T. H., and H. A. Weidenmüller, 1971, Phys. Rev. C **3**, 1856.
Smith, R. A., 1976, Phys. Lett. B **63**, 369.
Smith, R. A., 1977, Invited Talk at the Workshop on Nuclear and Dense Matter, May 3–6, University of Illinois, Urbana, Illinois.
Sprung, D. W. L., 1972, Adv. Nucl. Phys. **5**, 225.
Sprung, D. W. L., P. K. Banerjee, A. M. Jopko, and M. K. Srivastava, 1970, Nucl. Phys. A **144**, 245.
Van Kampen, N. G., 1961, Physica **27**, 783.
van Leeuwen, J. M. J., J. Groeneveld, and J. de Boer, 1959, Physica **25**, 792.
Wiringa, R. B., and V. R. Pandharipande, 1978, Nucl. Phys. A 299, 1.
Wong, C.-W., 1971, Phys. Rev. C **3**, 1058.
Wong, C.-W., 1977, Phys. Rev. C **15**, 1866.
Wu, F. Y., and E. Feenberg, 1962, Phys. Rev. **128**, 943.
Zabolitzky, J. G., 1974, Nucl. Phys. A **228**, 285.
Zabolitzky, J. G., 1976a, Phys. Lett. B **64**, 233.
Zabolitzky, J. G., 1976b, Phys. Rev. C **14**, 1207.
Zabolitzky, J. G., 1977, Phys. Rev. A **16**, 1258.